Development of FPGA-based multi-sensor excitation low voltage (MSELV) chassis at Jefferson Lab

P. K. Ghoshal (iD), R. Bachimanchi, P. Bonneau, P. Campero Rojas, B. J. Eng (iD), R. J. Fair, T. Lemon (iD), and N. R. Sandoval

View Online   Export Citation   CrossMark

Development of FPGA-based multi-sensor excitation low voltage (MSELV) chassis at Jefferson Lab

View Online   Export Citation   CrossMark

P. K. Ghoshal,[1,a] [ID] R. Bachimanchi,[2] P. Bonneau,[3] P. Campero Rojas,[3] B. J. Eng,[3] [ID] R. J. Fair,[1] T. Lemon,[3] [ID]
and N. R. Sandoval[4]

AFFILIATIONS

[1] Magnet Group, Experimental Nuclear Physics Division, Jefferson Lab, Newport News, Virginia 23606, USA
[2] Engineering Division, Jefferson Lab, Newport News, Virginia 23606, USA
[3] Detector Support Group, Experimental Nuclear Physics Division, Jefferson Lab, Newport News, Virginia 23606, USA
[4] Fast Electronics Group, Experimental Nuclear Physics Division, Jefferson Lab, Newport News, Virginia 23606, USA

[a] Author to whom correspondence should be addressed: ghoshal@jlab.org

ABSTRACT

The design and development of the sensor excitation and read back chassis was driven by the requirements for the monitoring and control of two conduction-cooled superconducting magnets in Hall B for the 12 GeV accelerator upgrade. The torus and solenoid superconducting magnets require extensive instrumentation. Sensor selection was accomplished by applying Jefferson Lab's (JLab) risk mitigation process, which employed a failure modes and effects analysis approach. The goal was to accommodate all sensor types for monitoring and control and to develop a generic multisensor excitation low voltage chassis that would be used across both magnet systems with a reduced set of functions. The chassis has been deployed in experimental Hall B at JLab and has been performing successfully since July 2016.

https://doi.org/10.1063/1.5127460

I. INTRODUCTION

As part of the Jefferson Lab (JLab) 12 GeV accelerator upgrade, the Experimental Physics Hall B detector system requires two superconducting magnets—a torus and a solenoid.[1] We describe the philosophy behind the instrumentation selection and control and data acquisition design, which accounts for several somewhat challenging working conditions. The magnet instrumentation system consists of a Jefferson Lab-designed multisensor-excitation-chassis that incorporates a Field Programmable Gate Array (FPGA).

Configuration, monitoring, and alarm handlers for the magnet systems are provided via an Experimental Physics Instrumentation and Control System (EPICS) interface. Failure Modes and Effects Analysis (FMEA) and the requirement to monitor critical parameters during operation guided the selection of instrumentation and associated hardware.[2] The successful commissioning and subsequent performance of these magnets demonstrates the

robustness of the design and implementation approach that was adopted by the Jefferson Lab team and serves as an excellent guide for future projects of this size and complexity.

Both magnet systems were subjected to a detailed Risk Assessment and Mitigation (RAM) process.[2] The process was used to evaluate the overall magnet system design as well as the robustness of each individual subsystem therein, including the instrumentation and control (I and C) subsystems. One critical component identified within this subsystem was the instrumentation readout electronics.

Guided by the system requirements and the need for high reliability, commercial off-the-shelf (COTS) readout boxes are available but usually possess only a limited number of channels. Furthermore, the multifunctional capability of these devices usually means that these devices are expensive. The torus and solenoid magnet systems require a wide variety of sensors and, therefore, require dedicated instrument readout boxes that can take up a lot of physical space in instrumentation racks. Additionally, we also needed

FIG. 1. MSELV—(a) the front panel of the chassis and (b) the back panel of the chassis (*each D-connector consists of 2-channels*).

to provide a fully synchronized interface (for both hardware and software) for the programmable logic controller (PLC) and EPICS subsystems and having to address multiple readout boxes might add to the complexity. The 12 GeV Project encouraged Controls and Instrumentation team to explore other alternative solutions. The secondary motivation was to extend the design to allow it to be made available for any general purpose measurement and services in the future.

We opted to develop a multisensor excitation low voltage (MSELV) chassis concept (Fig. 1). The concept design uses a fast FPGA-based system to accommodate up to 56 channels per chassis.

The development of the MSELV required that we addressed the following criteria for use within the experimental hall:

(a) Measurement quality—defines uncertainty, repeatability, resolution, and stability in comparison to a standard commercial readout box (for the identified sensors).
(b) Design of experiment—defines the operating range and control parameters.
(c) Installation and replacement—overall cost, ease of installation, ease of use, reliability, ongoing maintenance, support, and upgradeability.

In order to test and qualify each of the six torus coils for operation at cryogenic temperatures, the engineering team at JLab set up a test facility to allow each coil to be cooled close to 80 K.[3] This provided the team with an excellent opportunity to qualify most of our instrumentation for the coils as well as the first version of the MSELV.

The entire torus cold mass is supported by 3 axial supports (i.e., in the beam direction), 4 vertical supports, 2 lateral out-of-plane supports (OOPS) at the hub, and 24 coil OOP supports[4,5] (Fig. 2) mounted on either side of the torus Coil Cold Mass (CCM). The vertical supports take the gravity load for the 25 ton cold mass, while the axial supports react to any loads in the beam, pitch, and yaw directions and also support seismic loads. The OOPS assembly includes a room temperature load cell to monitor the out-of-plane

force, while the axial and vertical supports are stainless steel links with strain gauges (SG) mounted near the warm end. The load cells (LC) and strain gauges mounted on the magnet's structural elements were interlocked to the magnet power supply for a controlled run down via the PLC control system if any of the preset load thresholds were exceeded. The FMEA approach used also recommended that the loading on the cold hex beams and the hub should be monitored. The torus magnet was also extensively instrumented with multiple and redundant temperature sensors on the CCM and on the thermal shield at key locations.

Any sensor selected for use either on the magnet itself or within the cryogenic subsystem needed to be capable of operating reliably and repeatedly at cryogenic temperatures, in vacuum and in the presence of magnetic fields. These were the key drivers and led to the selection of the sensors listed in Table I (torus and solenoid). All other instrumentation (e.g., coil voltages, pressure, and cryogen levels) used a different set of electronics.[4]

Torus: each upstream hex beam contains 2-Cernox (CX) sensors (1 on the hex beam metal and 1 mounted to the coil splice inside the hex beam) as shown in Fig. 3. Each CCM has 11 Cernox sensors attached to the copper-cooling sheets potted with the winding [Fig. 4(a)], and each CCM also has 5 PT100 sensors attached to the thermal shield (4 on the back and 1 on the front), as shown in Fig. 4(b), in order to monitor the temperature distribution across each CCM.

Both the magnets within experimental Hall B are instrumented extensively, and readings are processed through their respective data acquisition subsystems (DAQ), to enable monitoring of the magnets and control their operation based on the data acquired.

II. DESIGN PRINCIPLE

The design of the sensor read back chassis was based on the requirements of the instrumentation for the torus and solenoid magnet systems, which in turn were guided by the output of the employed risk mitigation strategy.[4]
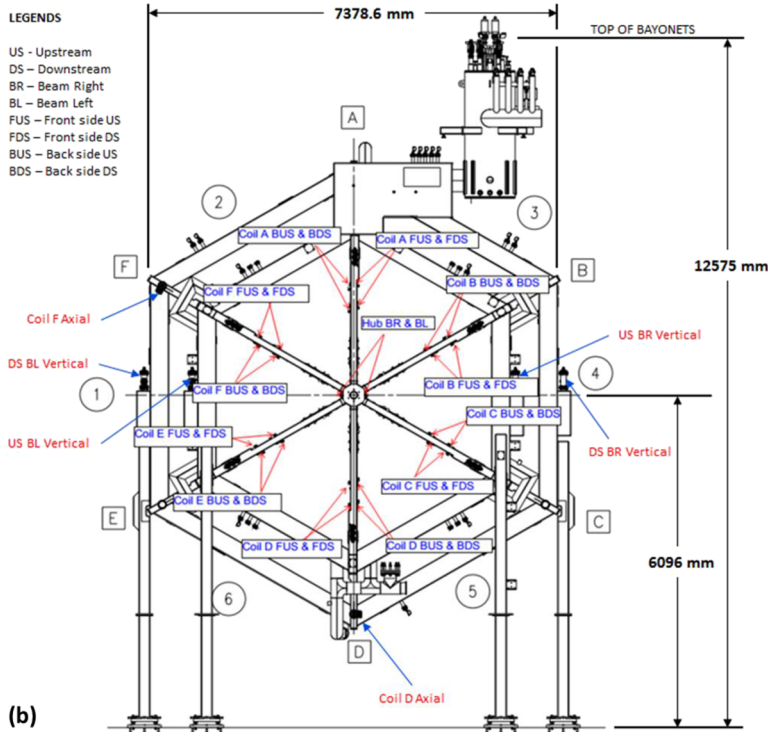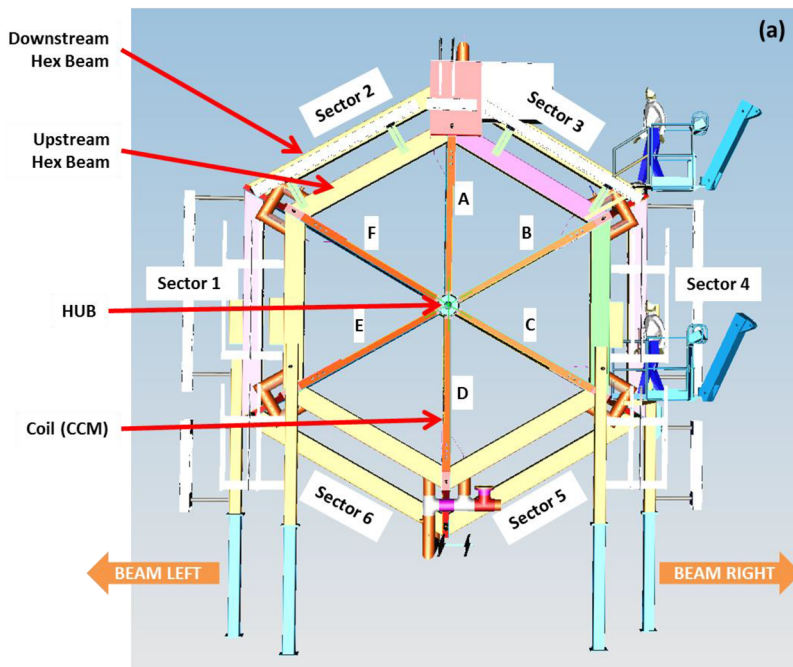
FIG. 2. Torus—(a) schematic showing the CCM, sector locations with respect to the beam direction, view looking down-beam and (b) support locations (axial, vertical, and OOPS).

The primary goal was to be able to read all the sensor types identified in Table I, which could then be fed to the control system for both magnets. These requirements led to a Jefferson Lab-designed and developed FPGA-based MSELV chassis. The chassis sets the excitation current or voltage for a sensor and provides read back, presently configured via a serial port. The data read back (in terms of voltage) would then be routed to a National Instruments Compact Real-time Input Output (NI-cRIO) unit (*cRIO-9074 for*

TABLE I. Magnet system sensors.

Measurement	Temperature (4.2 K)	Temperature (77 K)	Strain (torus)	Load cell (Torus)	Load cell (Solenoid)	Hall sensor
Sensor/wiring type	Cernox[TM][a]	Calibrated PT100[a] (Omega F2020-100-B)	Cryogenic series 350 Ω (CFLA-6-350)[b]	Load Cell—FUTEK FSH02239[a] (2000 LBS), 300 K	Load cell[a], 300 K (force)	Cryogenics Hall generator (axial), HGCA-3020[a]
Number of sensors/location	Magnet 54 + 26; Cooling tube 12; Splices 8; VCL in cryostat 4	Thermal shield 60 + 18; Current leads 4; Axial support 3; Vertical support 4	Coil cold mass (CCM) 24; Axial sup 6; Vertical sup 8; FMEA result 24 (hex)	OOPS 26; FMEA result 3 (hub)	8 (LCM307) 0–10 kN (axial); 8 (KMR300 kN) 0–165 kN (radial)	Vacuum vessel 6 + 3
Wire material	Constantan harness (twisted pair)	Constantan harness (twisted pair)	Constantan harness (twisted pair)	Copper (twisted pair)	Copper (twisted pair)	Copper (twisted pair)
Signal amplitude	3 mV (300 K) to 50 mV (4.2 K)	0.1 V (77 K) to 0.5 V (300 K), actual excitation current = 2.5 mA	0–5 V for resistance measurement, the variation is 0–0.5 Ω or 10 µV–1 mV (CFLA-6-350)	~2.0 mV/V		~1.00 mV/kG (at 298 K)
Sampling rate	>100 Hz	>100 Hz	>100 Hz	>100 Hz	>100 Hz	>100 Hz
Excitation current/voltage	0.20–20 µA	1–5 mA	0–10 V (2.5 V)	0–10 V (2.5 V)		100 mA
Multiplexed	Y	Y	Y	Y		Y
Control	PLC	PLC	PLC	PLC		PLC
Fast DAQ	FPGA	FPGA	FPGA	FPGA		FPGA

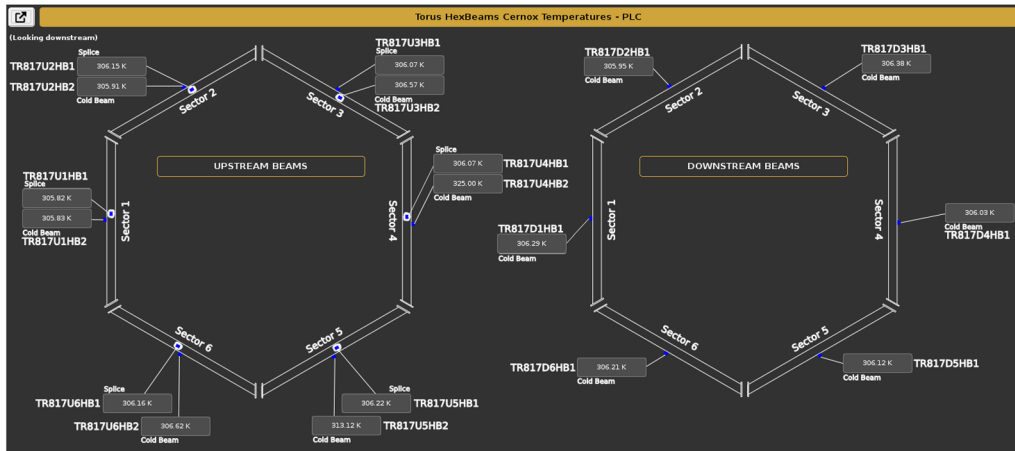[a]4-wire measurement.
[b]4-wire/3-wire for measurement.

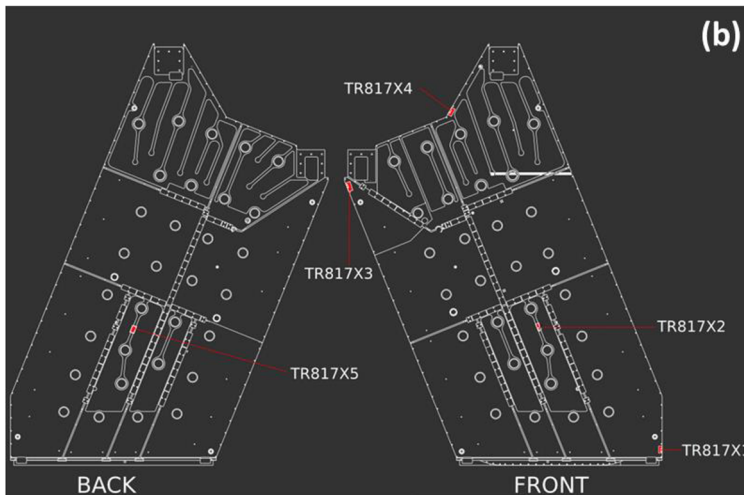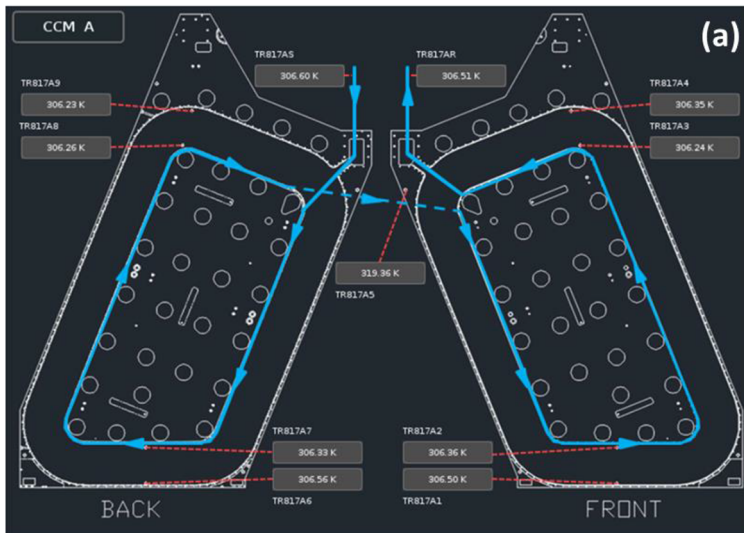**FIG. 3**. Torus magnet hex beam temperatures (Cernox sensors) are visible in EPICS.

FIG. 4. Torus magnet back and front sides of CCM showing the locations. (a) View of CCM temperature screen Cernox sensors in EPICS and (b) shield temperatures in EPICS nitrogen screen view of thermal shield temperature.
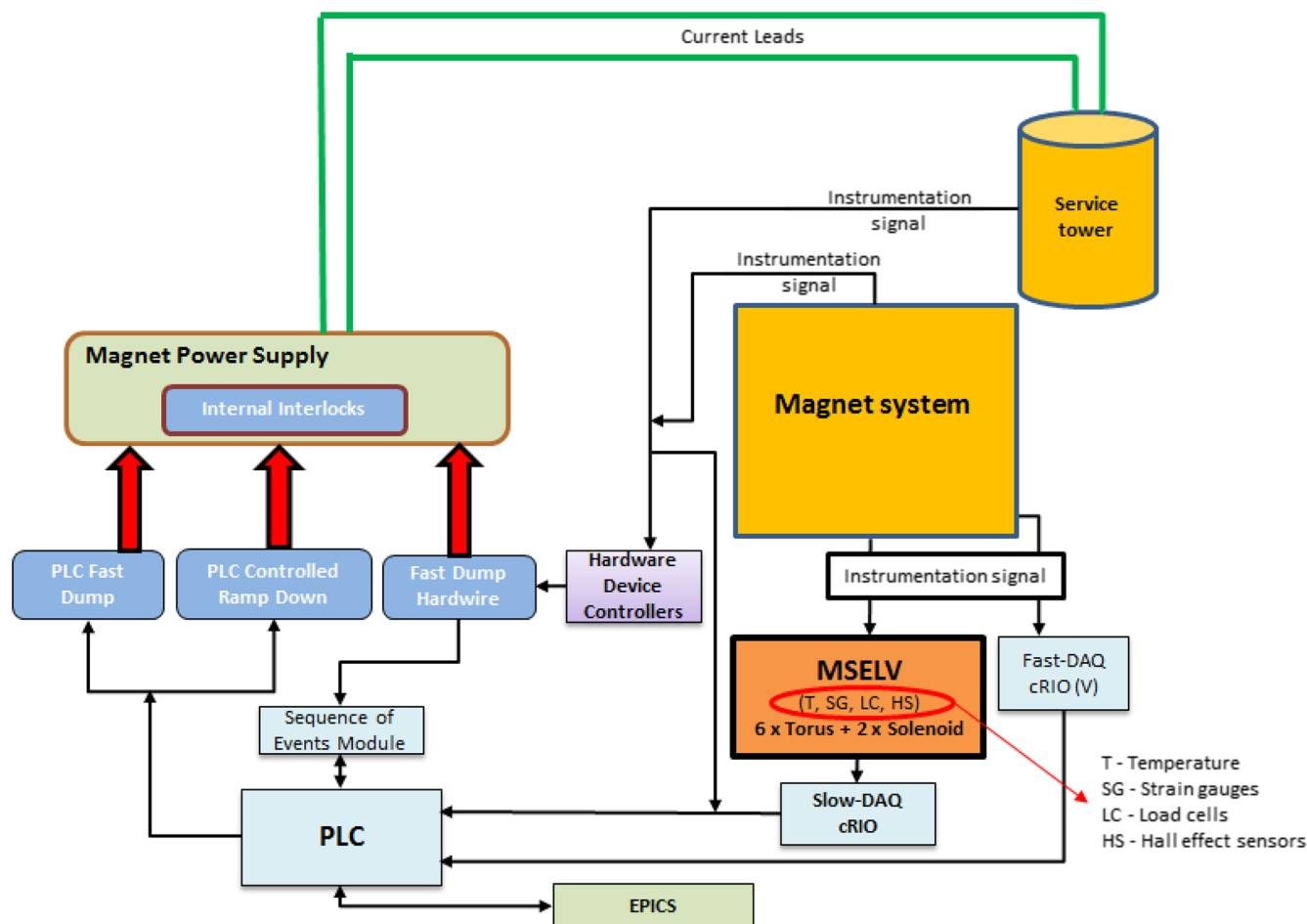
FIG. 5. Global architecture of the torus and solenoid magnet interlock system (MSELV—6 chassis for the torus and 2 chassis for the solenoid).

solenoid and cRIO-9030 for torus), also known as the slow DAQ system, which would in turn pass data to the PLC for the control of the various subsystems and interlocks (Fig. 5).

Prior to designing the MSELV system, a smaller FPGA-based system had been developed earlier for superconducting radiofrequency (SRF) cavities at JLab using analog-to-digital convertors (ADCs) and digital-to-analog convertors (DACs). With some modifications to this smaller version, a development MSELV unit, with a limited number of channels, was built for the 80 K test for the torus coils.[3] With the experience gained from the 80 K test, a more complete chassis accommodating all 56 channels was designed to suit the needs of both the torus and solenoid magnets.

Typical magnet instrumentation wiring and termination diagrams for the torus magnet for OOPS load cells, strain gauges, PT100, Cernox sensors, and magnetic field Hall sensors are shown in Figs. 6 and 7.

EPICS screenshots showing actual temperature readouts (Cernox and PT temperature sensors) and load cells for the torus and solenoid magnets prior to magnet energization are shown in Figs. 8 and 9.

III. HARDWARE

The MSELV chassis consists of different boards for temperature sensors (both 4 K and 77 K), load cells, and strain gauges and covers the following:

(a) Voltage-in voltage-out board along with a voltage-in current-out board with current output range of 200 nA–20 μA is used for Cernox (CX) sensors and is based on a precision voltage to current converter application.

(b) Voltage-in and current-out board with current output range between 1 mA and 5 mA is used for PT100 (Platinum-100) sensors.

(c) Voltage-in and voltage-out board is used for Strain Gauges (SG) and Load Cells (LC).

Table II shows the sample range of the resistance values of different Cernox sensors at four different temperatures from
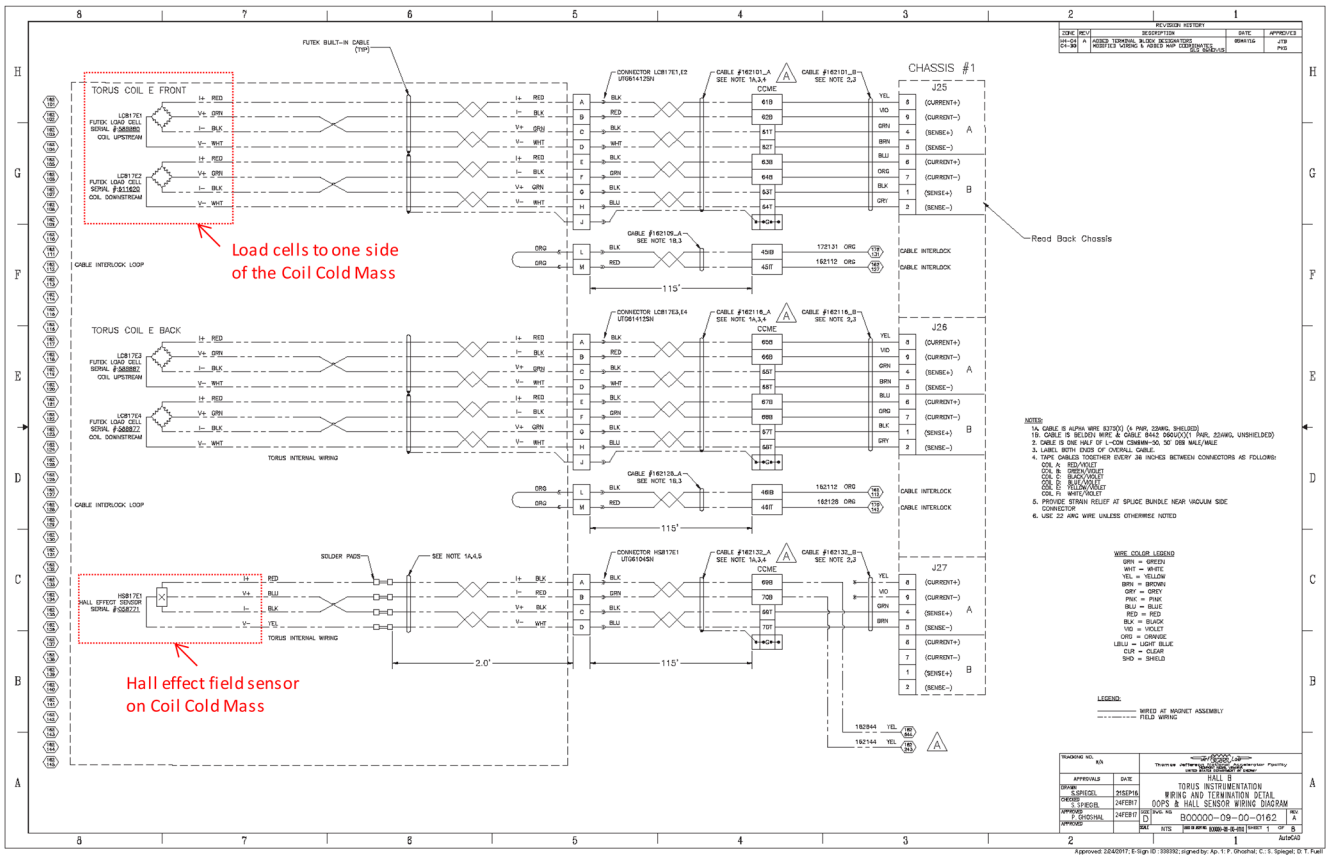
FIG. 6. Typical torus instrumentation wiring and termination details for the out-of-plane supports (OOPS) and Hall field sensors.

Lakeshore®. The maximum power dissipation allowed across the Cernox limits the temperature rise to no higher than 1.0 mK, as recommended by the sensor manufacturer.[6] A maximum allowable excitation current is thus calculated for each sensor at defined temperatures and is given in Table II, where the exciting current can vary from 380 nA to 141 μA. As the accuracy of the measurement from room temperature down to liquid nitrogen is little flexible (± 0.5 K ≤ 100 K to ± 2 K > 100 K), an excitation current of 20 μA was selected for this range. As we get closer to the 4.2 K point, accuracy becomes more important (± 50 mK) and so the excitation current range at lower temperatures was selected to be 200 nA to 20 μA. Software running on the cRIO continuously calculates the power dissipation and adjusts the excitation current accordingly.

Error mitigation - The algorithm would encounter an unknown state when switching between different temperature ranges. To mitigate this effect, the excitation current below 10 K was fixed to 400 nA. The excitation current calculation was thus simplified, and there was no subsequent concern about exceeding the maximum allowable power dissipation limit as the resistances of all the Cernox sensors on both the torus and the solenoid fell within the required range.

The boards for strain and load measurement and PT100 temperature sensors use the same printed-circuit-board (PCB) design with a few changes to the values of resistors. This approach simplifies the design, avoids having to design two different boards, and also makes future maintenance and upgrades easier, thereby complying with a key requirement for the 12 GeV upgrade project.

The circuit for voltage read-back used instrumentation amplifiers.[7] All design variations adopted by JLab are based on applications of operational amplifiers, ADCs, and DACs. The DAC (DAC8568) and ADC (ADS1258),[7] both from Texas Instruments (TI), are used to drive voltage/current and voltage read-back across the sensors, respectively, together with an operational amplifier. The circuit shown in Fig. 10 is a modular design for the prototype module designed and tested using INA2141 with fixed gains on this instrumentation amplifier (fixed to either 10 or 100) used for reading the voltage from a sensor.[8] In order to add flexibility to the production version, different gains are required for different sensors (e.g., *51 for Cernox, strain gauge, load cells with 1 kΩ resistor, and 6 for PT100 with 10 kΩ resistor*) and also the variation in gain due to the internal resistor. The INA2128 instrument amplifier has been used during the production of the MSELV. Both INA2128 and
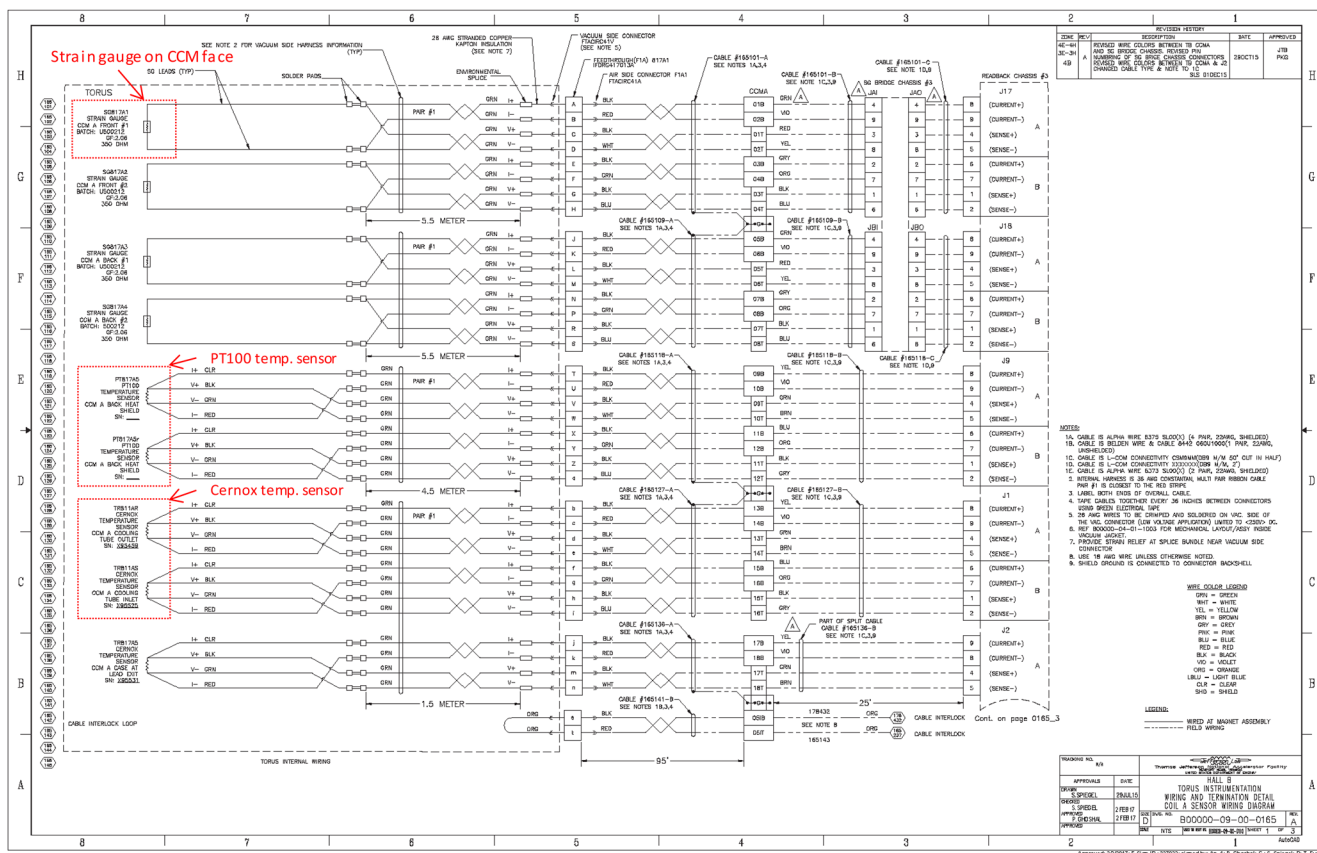
FIG. 7. Typical torus instrumentation wiring and termination details of one torus magnet coil—strain gauges, PT100, and Cernox sensors.

INA2141 instrumentation amplifiers are pin compatible, hence, no design changes were needed. An instrumentation amplifier with a common mode rejection filter is used because this circuit makes sure the lead resistance is canceled out for the differential measurement. Output of the amplifier is fed to the input of an ADC for reading through the FPGA. A test point is added on the board at the output and is used for debugging the board or for looking at a signal using an oscilloscope. The gain of the instrumentation amplifier is set based on the type of sensor. Gains are selected in such a way that only the PT100 circuit has a different gain from all the other sensors. This also helps when assembling the board, since all the boards are modular, and minimal changes are, therefore, needed.

A commercial FPGA board[9] is used for communicating with the ADCs and DACs. This FPGA communicates with the NI-cRIO, which is a real-time embedded industrial controller based on a FPGA by National Instruments via an RS232 interface. A PCB was designed by JLab to route signals to the different boards via RS232 communication with the NI-cRIO. All the boards were prototyped and underwent extensive test cycles including testing with multiple-sensors and different types of sensors in various combinations before going into a full production cycle. This final

design of the chassis was based on the experience gained from extensive testing at 80 K and subsequently at 4.2 K during the development process at JLab. A total of six chassis for the torus and two for the solenoid are employed for the overall instrumentation and control subsystems.

A DE0-Nano[9] board from Terasic with an Altera Cyclone IV FPGA is used to communicate with the ADC and DAC using a Serial Peripheral Interface (SPI) protocol. The NI-cRIO acts as a master and communicates with the FPGA over RS-232 that sets the excitation voltage or current required and reads the voltages back, which subsequently are converted into engineering units.

The design philosophy behind the chassis is to make the system for easy access and readout in EPICS by having

1. a FPGA module and program,
2. readout modes for the Cernox based on versatile logic of power (*as commercial manufacturers do*),
3. strain gauges and load cells test and readout, and
4. common/modular schematics/program for easy trouble-shooting.

The function of the modules and ports in MSELV are shown in Fig. 11 as follows:
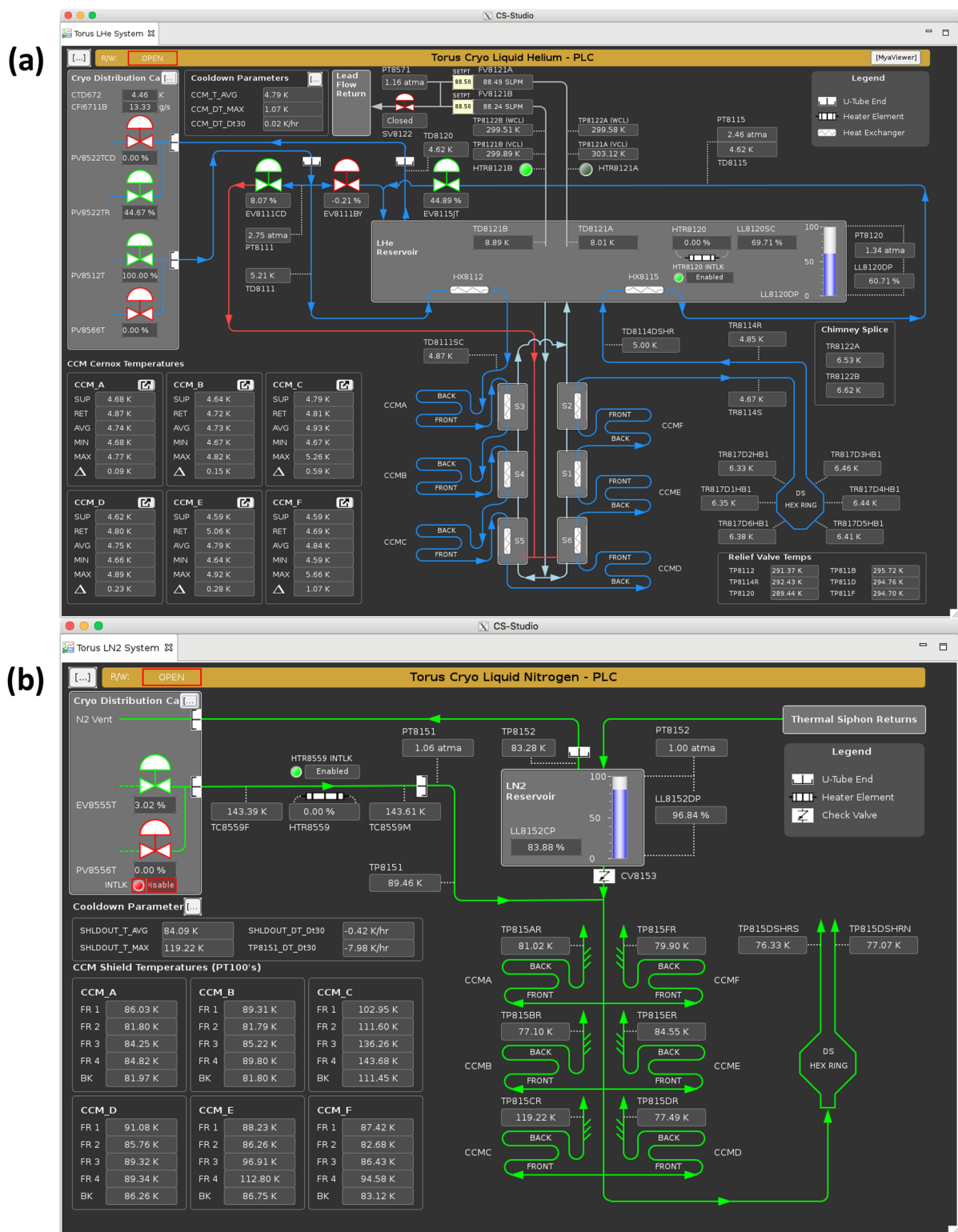
FIG. 8. Screenshots from EPICS showing temperatures of the torus magnet—(a) liquid helium and (b) liquid nitrogen circuits (using Cernox and PT temperature sensors, respectively) prior to magnet energization.
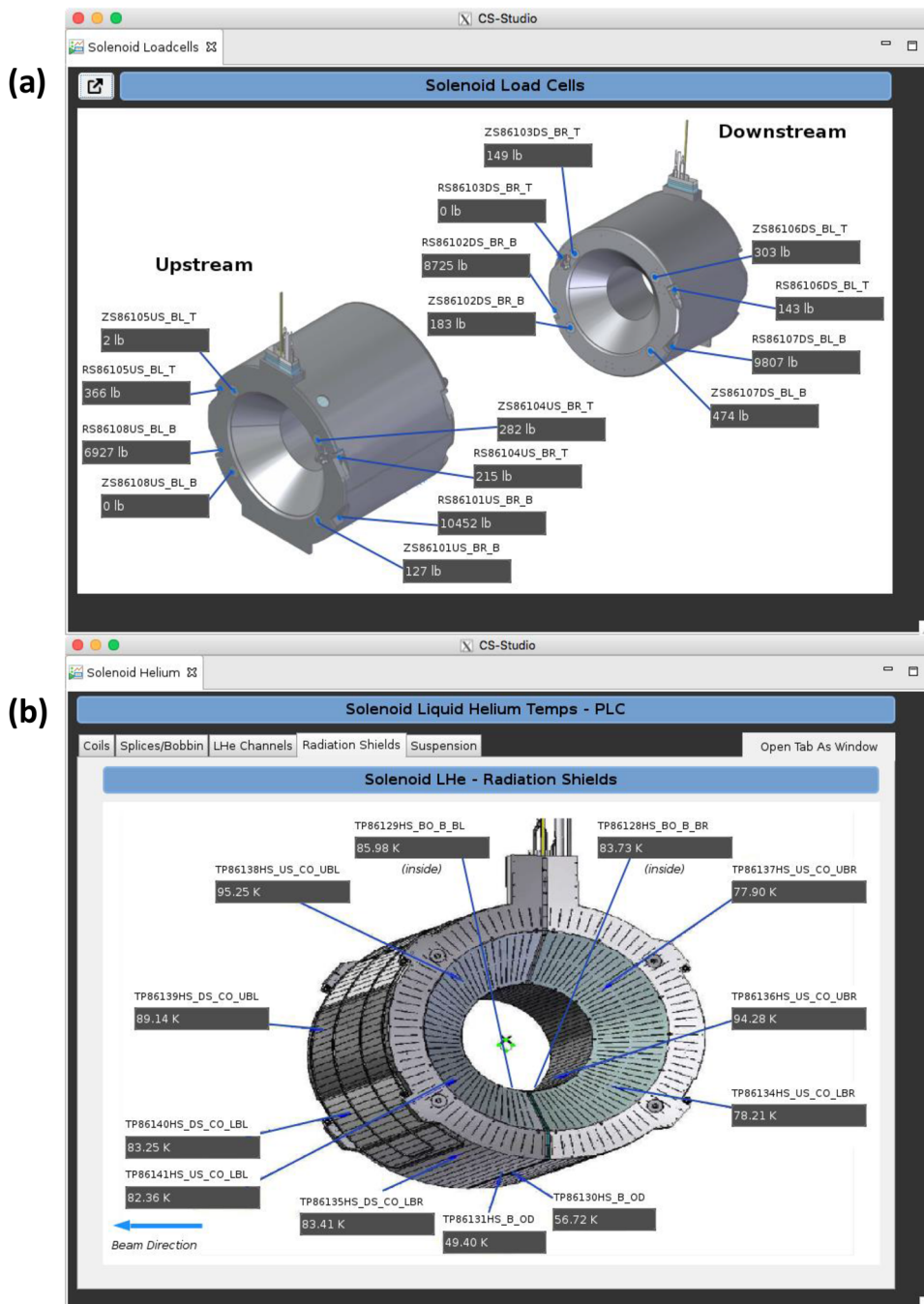
FIG. 9. Screenshots from EPICS showing temperatures for the solenoid magnet—(a) load cells and (b) thermal shield temperature distributions prior to magnet energization.

- *CX $V_{in}V_{out}$*—reads up to 16 channels, sets the voltage to CX $V_{in}I_{out}$ to generate excitation current, ADS1258 (ADC) for reading, and DAC8568 (2x DAC) to set the voltage.
- *CX $V_{in}I_{out}$*—generates the excitation current based on the input voltage, precise and low drift circuit from LT1167[10] in Fig. 12, and a precision voltage-to-current converter.
- *PT $V_{in}I_{out}$*—same PCB as CX $V_{in}V_{out}$ and two resistor changes to make the board generate excitation current.
- *SG $V_{in}V_{out}$*—same as CX $V_{in}V_{out}$.

TABLE II. Required maximum excitation current for the three types of Cernox sensors for temperature measurement.

		Resistance of the Cernox (Ω)					
Temp (K)	Max. P_{diss} (μW)	Cernox: type 1	Max. current (μA)	Cernox: type 2	Max. current (μA)	Cernox: type 3	Max. current (μA)
300	1	50	141.00	100	100.00	150	81.60
77	1	500	44.70	800	35.40	1 000	31.60
10	0.1	1500	8.16	8000	3.54	15 000	2.58
4.2	0.01	3500	1.69	20 000	0.71	70 000	0.38

- $LC\ V_{in}V_{out}$—same as CX $V_{in}V_{out}$.
- Power supply, as shown in Fig. 13, provides ±12 V and +5 V to the power filtering and breakout board.

The circuits for setting up the excitation current for PT100 and excitation voltage for the other sensors are shown in Fig. 14. The modular design of the circuit is used to provide output that can be set to either voltage or current by changing resistors, providing the flexibility in design for all sensor types. Since the operational amplifier is used in the feedback, any changes across the cable/sensor are compensated for, and the sensor gets only the applied/requested excitation voltage or current (Figs. 15 and 16).

A DAC is used to set the excitation voltage and current, as shown in Fig. 17, with operational amplifiers. Since the DAC alone cannot provide enough excitation power to all the sensors, additional operational amplifiers are added.

Cernox sensors require very low excitation currents, of the order of nanoamperes, so selecting the appropriate current-driving circuit is critical, as illustrated in Fig. 12, which generates currents of about 200 nA. This uses the voltage output from the CX $V_{in}V_{out}$ board and drives the input to generate the required excitation current. The return current signal from the sensor is fed back to an operational amplifier. Voltage output of the operational amplifier, equivalent to the excitation current, is then fed to an ADC (Figs. 15
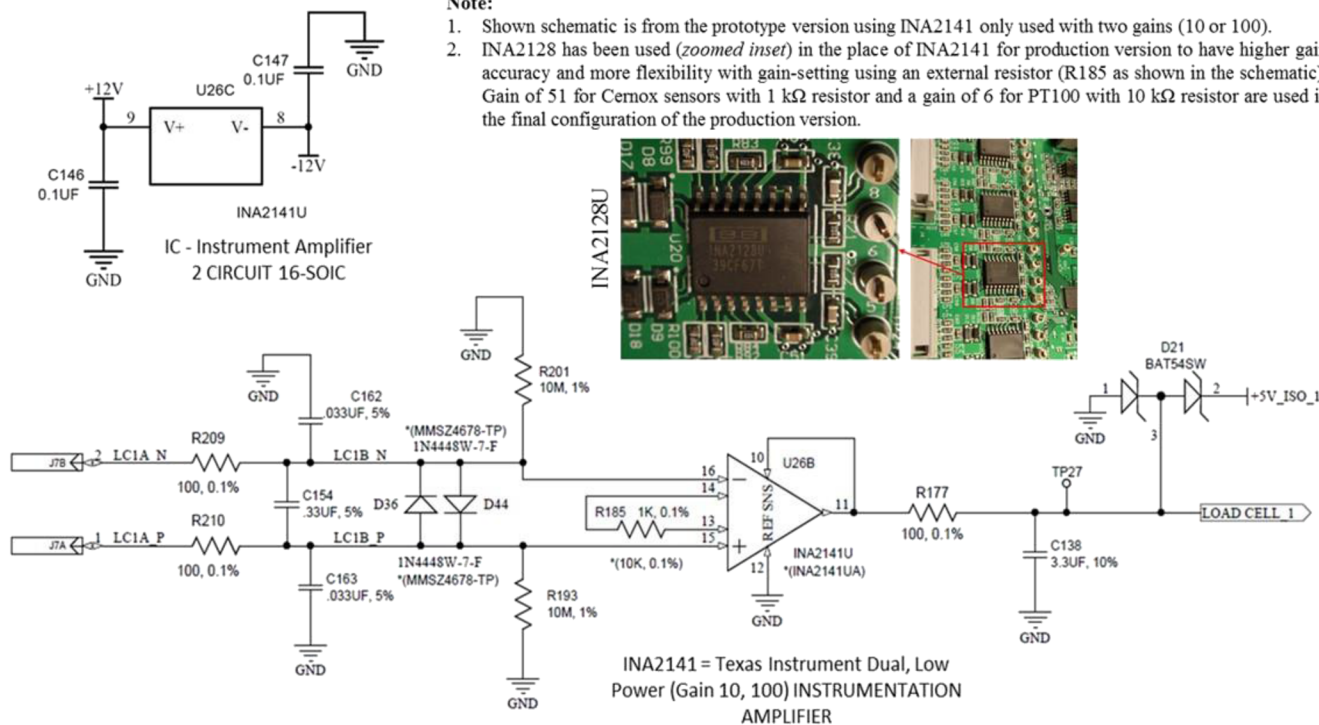

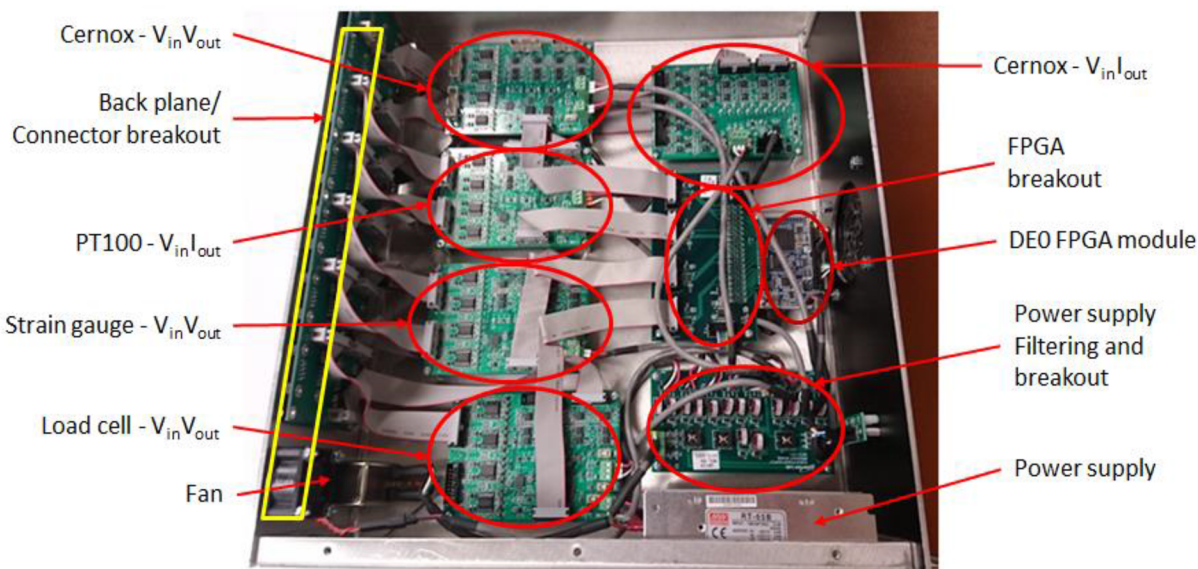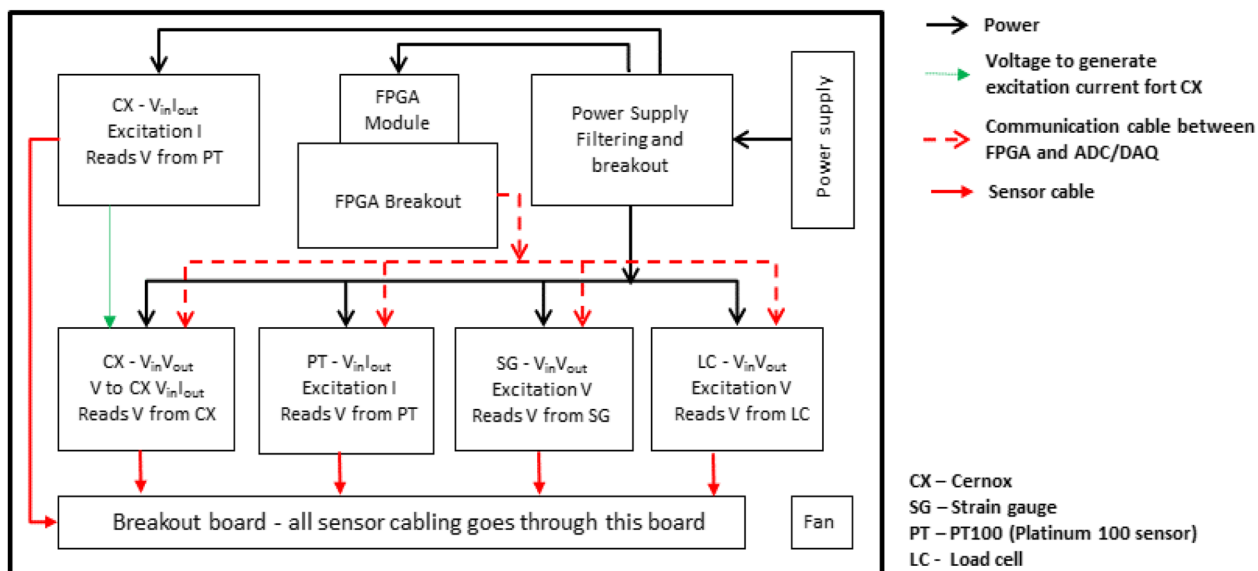FIG. 10. Typical modular circuit used for reading channel voltage.

FIG. 11. Typical layout of the board configuration inside the MSELV chassis.

and 16). In doing so and by monitoring the voltage output, any discontinuities in the cable can be easily detected. Presently, this functionality has not been included, but the system hardware has been prepared to allow future adoption. Both firmware and software will require some level of modification in order to add this functionality.

IV. FIRMWARE/SOFTWARE

Basic function read back all sensors - The excitation voltage for strain gauges and load cells can be adjusted from 0.5 V to 10 V.

This feature was useful during the debugging/commissioning phase to verify that the readings were linear with increasing excitation voltage. Once the debugging and the verification was completed, excitations were set to 2.5 V for strain gauges and 5.0 V for load cells.

All the read back channels are used with an analog filter operating at 200 Hz, and the voltages are sampled at 2 kHz. Filtering and sampling were fixed at these values. The analog filter can be modified, and the sampling frequency can be increased up to a maximum of 23 kHz per channel, adding flexibility to the system.
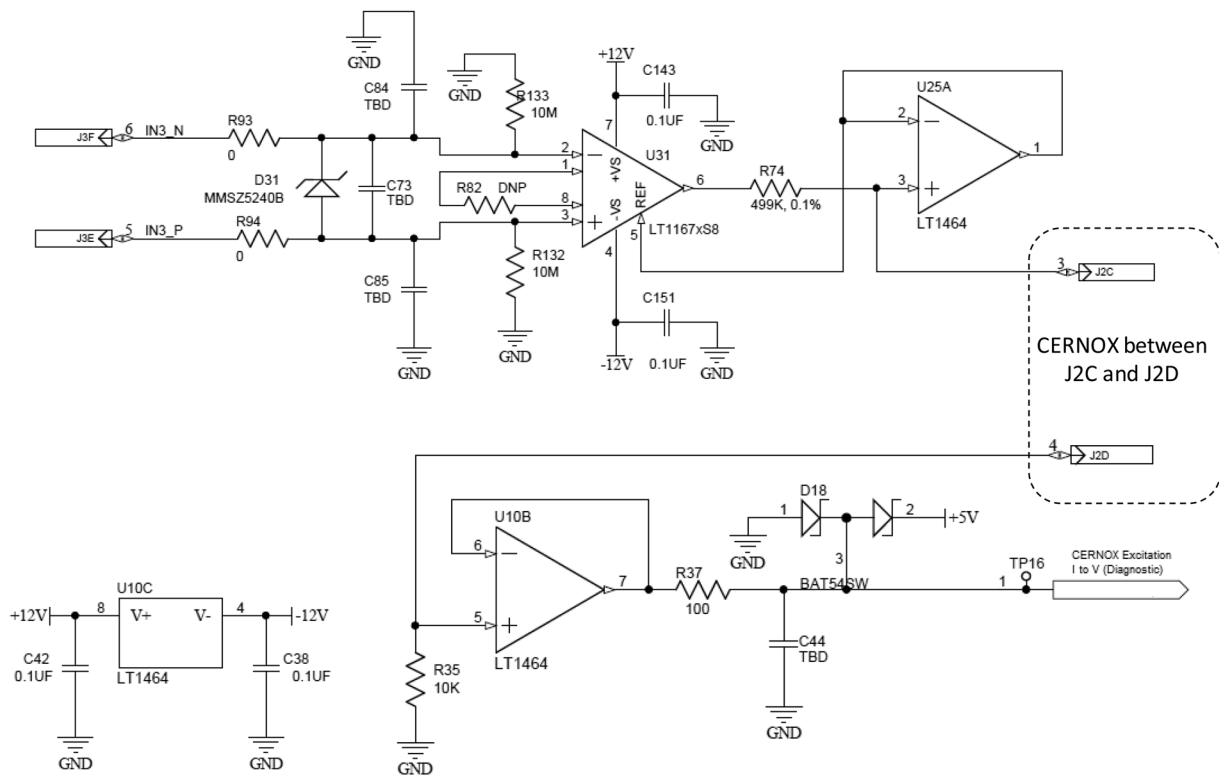
FIG. 12. Typical circuit for generating the low excitation current required for Cernox sensors.
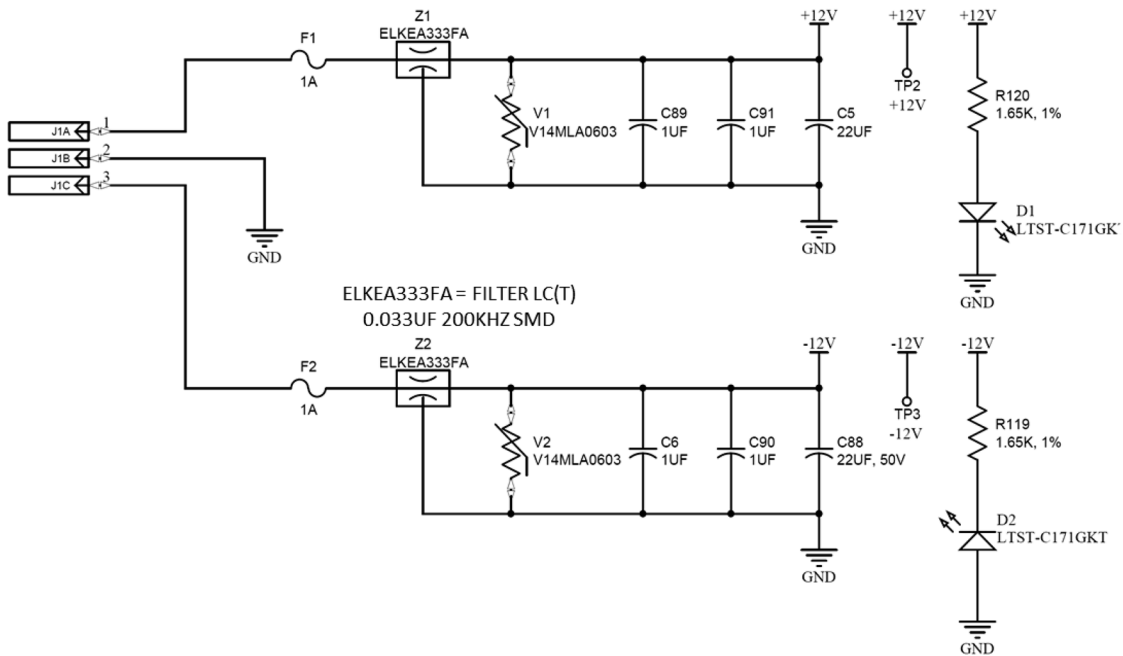
FIG. 13. Power supply module—for power filtering and breakout.
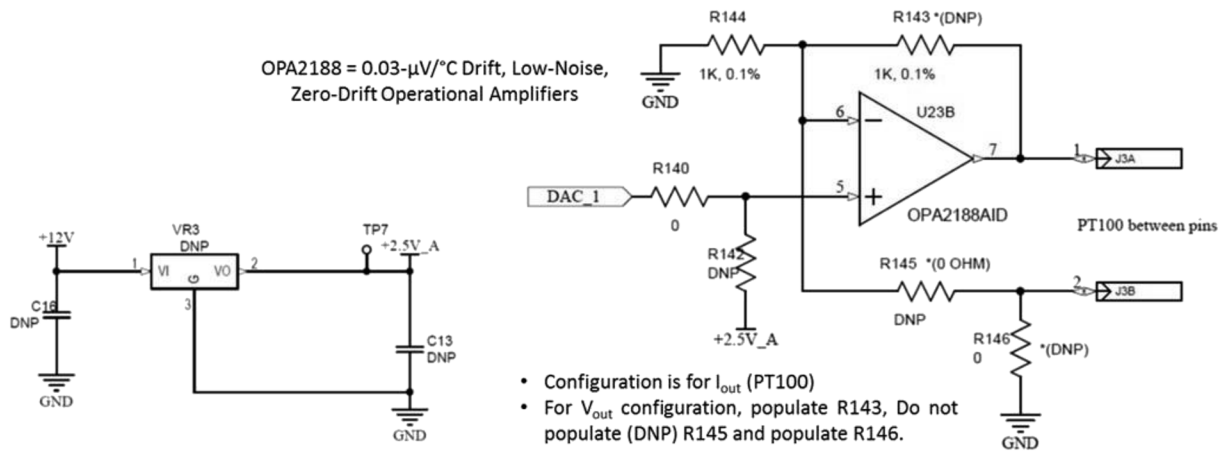
FIG. 14. Schematic diagram for sensor read back V_{IN}/V_{OUT}.

This helps in combining different types of sensors into one chassis, which is often required for a system (e.g., magnet instrumentation). The FPGA handles the setting of the excitation current and the read back from the channels with a simple RS232 interface that can be connected to any computer, which then allows for the offline analysis of the data.

The NI-cRIO is used as the bridge between the MSELV and the PLC. The hardware consists of both cRIO controller and NI-9780
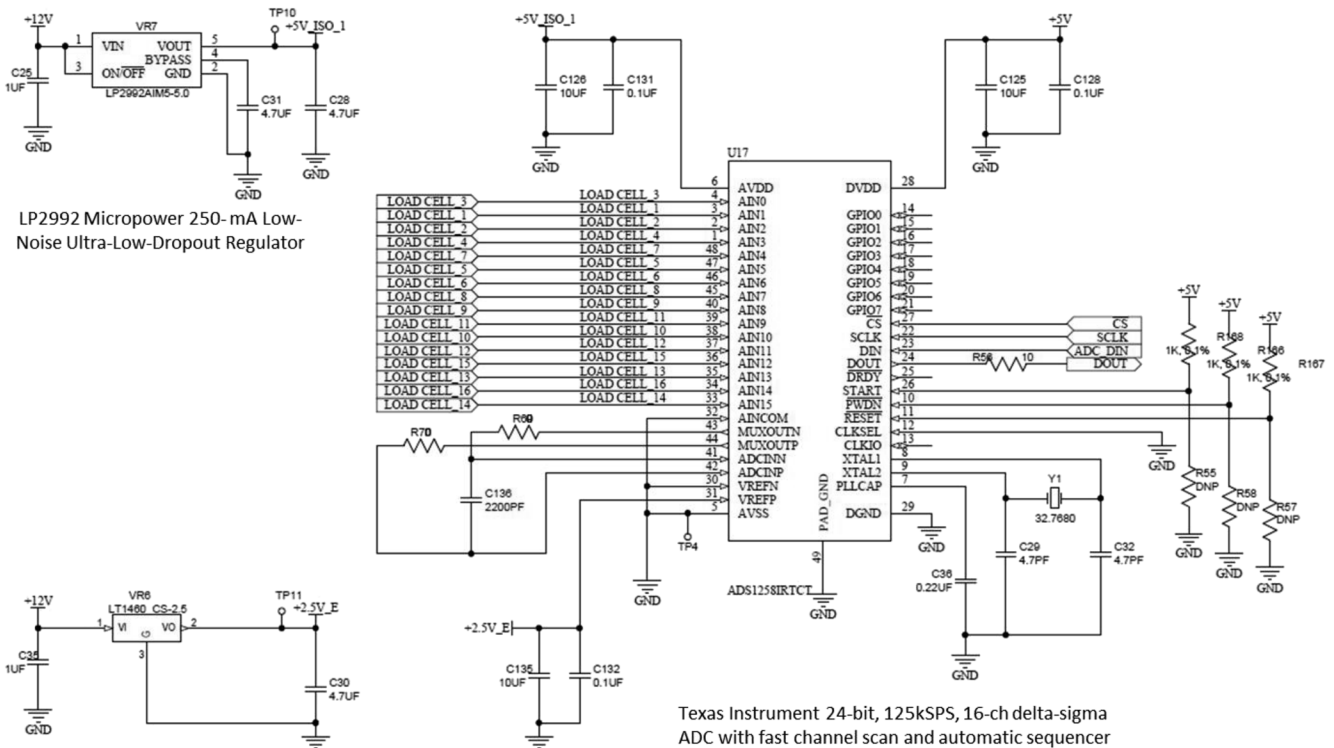
FIG. 15. Typical wiring layout for the instrumentation amplifier and outputs to the ADC.
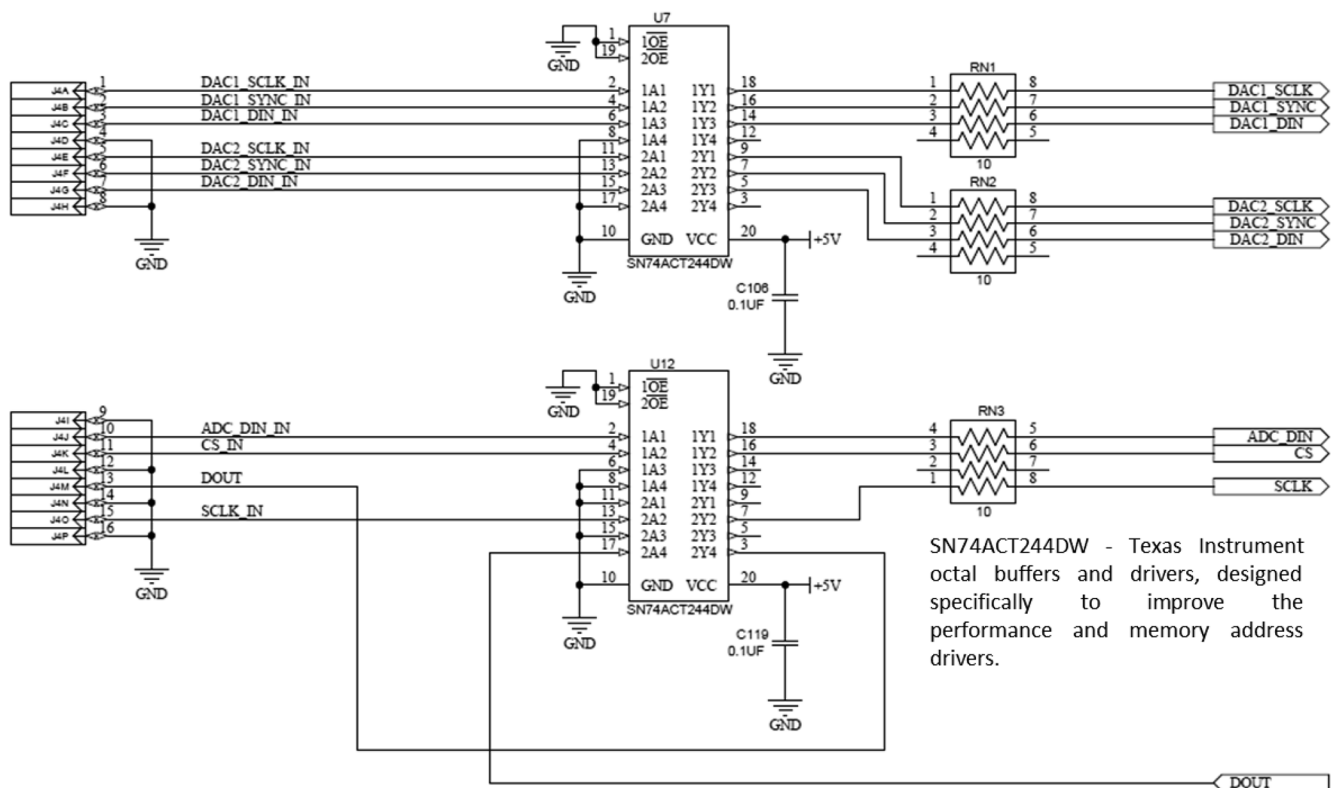
FIG. 16. Buffers translating the voltage between FPGA and ADC/DAC.

serial modules. The LabVIEW graphical programming language is used as the development environment to program the cRIO. The software is compiled as a real-time application and deployed on the cRIO to run on startup to do the following:

1. initialize the MSELV serial port;
2. setup the sensors connected to the chassis:
   (a) type of sensor,
   (b) initial excitation voltage, and
   (c) serial number;
3. readout all the sensors on the chassis based on type, e.g.,
   (a) load cells—interpolation based on calibration data for each individual load cell identified by serial number,
   (b) strain gauges,
   (c) PT100 sensors: convert resistance to temperature based on calibration data for each individual sensor identified by serial number,
   (d) Cernox sensors: differential readout, interpolate temperature based on calculated resistance from calibration table for each sensor identified by serial number and calculate new excitation, and
   (e) Hall effect sensors;
4. send sensor data to PLC via EtherNet/IP.

Steps 3 and 4 are in a loop that runs at 1 Hz.

The cRIO system's primary function is to convert the readings from the MSELV to values with units based on the sensor type and pass that data to the PLC. The following reasons guided our choice to use the cRIO—(a) difficulty in communicating with multiple serial ports on the PLC, (b) the need to allow for parallel development, and (c) NI cRIO systems are already used successfully and extensively across JLab. *However, there is no reason that it has to be a cRIO system*. Therefore, one of the upgrades available to the FPGA board is a newer model that is pin compatible and features a System-On-Chip (SOC) that runs Linux, which will allow the MSELV to directly communicate with the PLC via EtherNet/IP.[11] There are many implementations of this protocol (*Python* packages, OpENer, etc.) available on Linux. Deploying the upgraded FPGA would allow the elimination of the cRIO system, which would remove one potential point of failure, while also opening up additional feature sets (*integration into standard IT system monitoring, advanced logging, etc.*) due to running Linux.

V. MEASUREMENT PRINCIPLE AND EXPERIMENTAL SETUP

The test setup to enable the verification of the measurement and calibration using the development MSELV (beta-system) chassis was performed as follows:
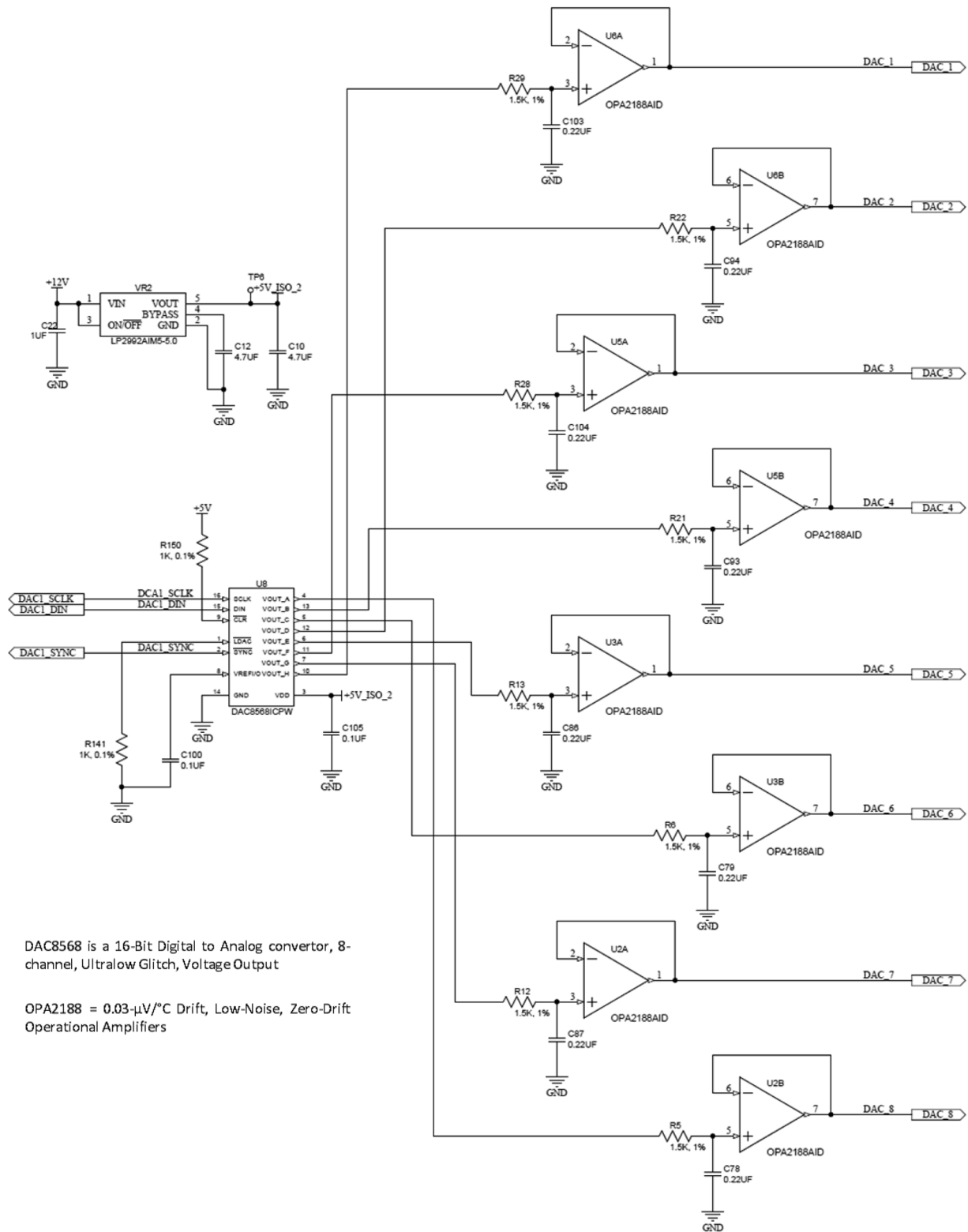
FIG. 17. Operational amplifiers for driving excitation voltage and current.

1. Beta/development system test—Liquid Nitrogen (LN_2) test.
2. Test Cernox and PT100 in LN_2 and Liquid Helium (LHe).
3. Tests at 4.2 K (Cernox) in vertical test facility (VTF).
4. Load test carried out on the supports.
5. Load and strain tests carried out with a strain gauge at LN_2 temperature.

Verification of Cernox sensors - Two separate tests were carried out on the sensor by cooling it down very rapidly and very gradually from room temperature to liquid nitrogen temperature. Verification was performed by comparing the output from the MSELV against a standard Lakeshore 216 temperature readout box. This test was carried out with multiple sensors mounted on a copper board (Fig. 18). This was repeated at least 5 times to verify the stability of performance. The circuit used for testing the Cernox was used across different chassis during the final test prior to prototyping. This circuit was finally used during the cold test of all 8 torus coils (6 actual +2 spare) from room temperature to 80 K. Following the results, test and verification was carried out at 4.2 K (in LHe) in one of the vertical test facility (VTF) dewars at JLab. The VTF has liquid helium at 4.2 K where multiple Cernox sensors were slowly lowered into liquid helium. The readout from the MSELV was recorded at different levels of excitation currents and was shown to have a variation better than 50 mK. The range of sensors that were selected for the test varied between 20 kΩ and 70 kΩ at 4.2 K.

Verification of PT100 sensors - PT100 sensors were submerged in liquid nitrogen, cross-calibrated against a calibrated Cernox sensor, and the values were read and recorded using both the MSELV and a Lakeshore 216 temperature readout box.

Verification of strain gauges and load cells was carried out in two steps. First, a known load was applied to the load cell, and the output was read out using a commercially available calibrated Futek® instrument.[12] The same procedure was then repeated using the MSELV as the readout box. The values read out by Futek and MSELV were reviewed, and the error between the readings was deemed to be acceptable.

VI. CALIBRATION AND TEST

Each production MSELV chassis underwent stringent tests and calibration procedures before being released for use in the hall. The tests included

(a) measuring predefined sensors to confirm the accuracy, stability, and repeatability of the measurement;
(b) a review and examination of potential failure modes; and
(c) a comparison of the output from the chassis with another standard calibrated measuring instrument.

The required sensor accuracies are provided in Table III. The accuracies used for the overall system measurement with the MSELV are based on the end value as monitored (which includes measurement, conversion, with all inaccuracies/errors, etc.).

Most COTS individual measuring instruments have specified accuracies, which are better than that required in order to achieve the overall accuracy required for the whole interlinked system. For the requirements specified within the experimental hall, for the identified applications, the MSELV is primarily required to provide readings reliably and accurately (i.e., for overall
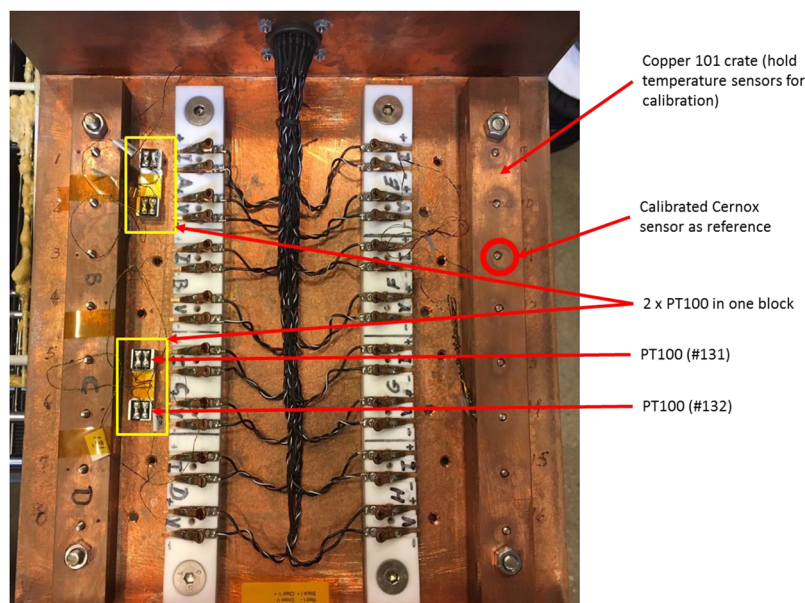
FIG. 18. Copper crate (housing) to hold temperature sensors (both PT100 and Cernox) for 4-wire calibration.

TABLE III. Acceptable tolerances in measurements.

Sensor type	Normal value	Tolerance
Cernox®	4.2–325 K	0.05 K (4.2–10 K) and 0.1–1 K (>10 K)
PT-100	50–400 K	0.5–2 K (50–400 K)
Load cells-FSH02239	0–2000 lbs	±10 lbs (2.0 mV/V)
Load cells-LCM307	0–10 kN	±50 N (2.0 mV/V)
KMR300 kN	0–165 kN	±50 N (2.0 mV/V
Hall sensor HGCA-3020	0–3 T	1.00 mV/kG (at 298 K)

accuracy) as detailed in Table III. Based on the measurements carried out, empirical equations with an estimated error bar were developed.

A. Strain gauges

Cryogenic strain gauges (CSG), type-CFLA-6-350 compatible at 4 K operation were used throughout the system.[13] CGS were employed for both 4 K and room temperature measurement on the vertical and axial supports in the torus magnet. The stainless steel axial support (to support loading in the beam direction due to misalignments or seismic motion) and vertical support links (to support the gravity load of the cold mass) were used to connect the cold mass to the vacuum jacket. A Wheatstone bridge circuit chassis is used upstream of the MSELV chassis for strain gauge measurement. It incorporates the strain gauge element on one arm,

Strain Gauge #1

Strain Gauge #2

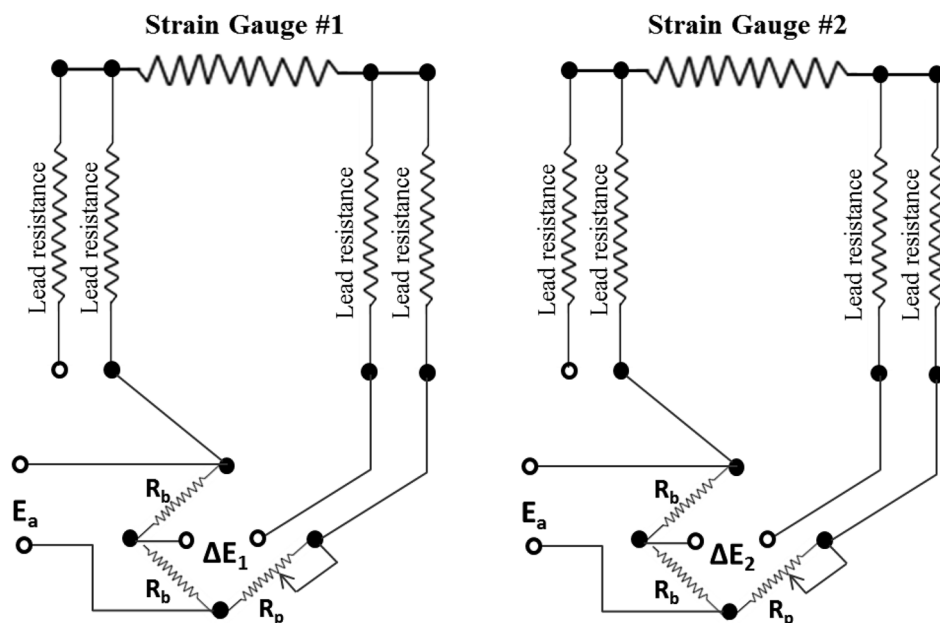**FIG. 19**. Wiring schematic showing the dual strain gauge (3-wire configuration).

E_a = Excitation voltage (V)
R_b = Precision bridge resistor (Ω)
R_p = Precision bridge pot resistor (Ω)
ΔE = The differential unbalanced voltage measured
Note:
- All resistors have tolerance < 0.1 %
- 3-wire measurement (prepared for 4 wire wiring)
- 2 strain gauges across 1 × 9-pin -D connector in MSELV

with the other arms utilizing high tolerance resistors as shown in Fig. 19. The system is passive, and all required excitation voltages are provided by the MSELV. The MSELV chassis works in conjunction with an ADC to only allow positive voltage values, thus forcing the bridges to always be balanced high, thus ensuring that all the read backs are always positive. The gauges are preassembled on the supports and calibrated prior to the installation as shown in Figs. 20 and 21.

A detailed test was carried out to evaluate MSELV performance under extreme conditions with strain gauges when exposed to (a) LN2 and (b) breaking force at room temperature. A typical test setup is shown in Figs. 22 and 23. A section of an epoxy-potted superconducting coil wound using actual Rutherford cable soldered into a copper c-channel was subjected to an increasing cantilevered load, and coil failure (cracking) was visually monitored
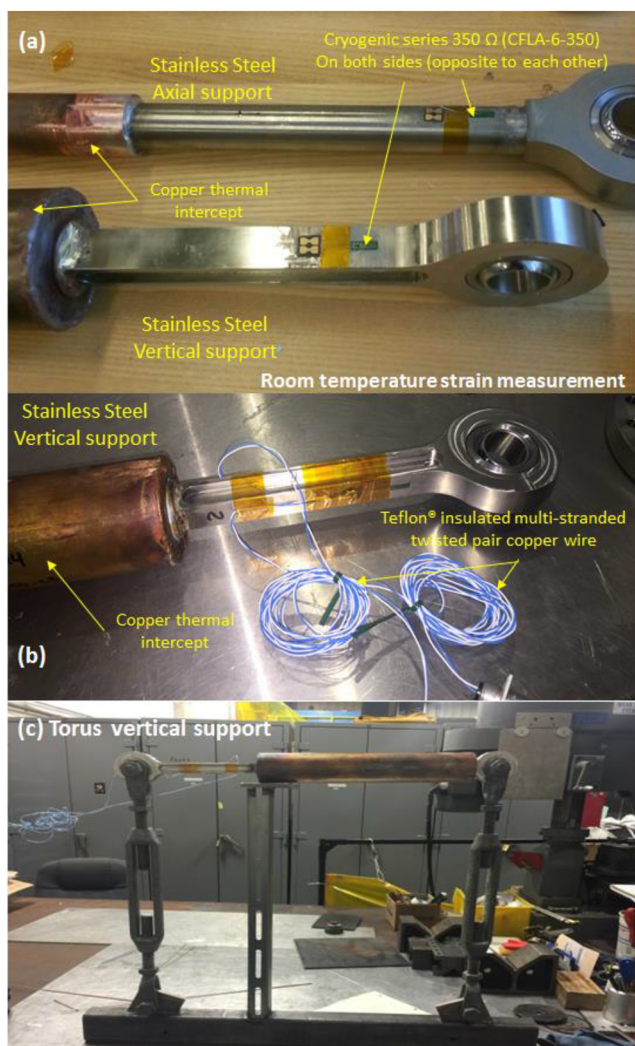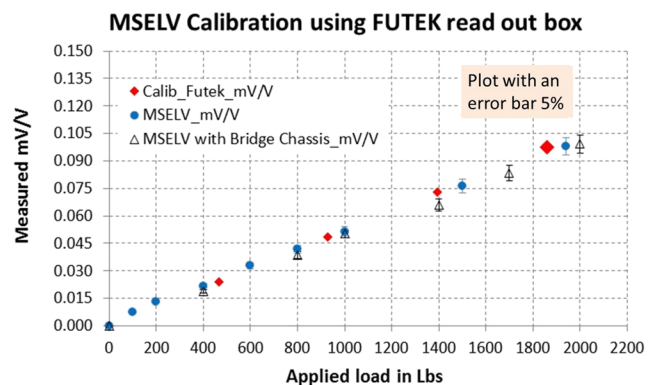

FIG. 21. Cross calibration of MSELV for load and strain gauge readout on axial support (having 2-CLTS strain gauges) against a standard calibrated readout box from FUTEK.

and correlated with collected data from the strain gauges (Figs. 24 and 25).

B. Load cells

Load cells were evaluated "live" in the system during commissioning and an engineering run prior to the start of the actual physics experiment. A worst case scenario involving a solenoid magnet fast dump was fully evaluated.
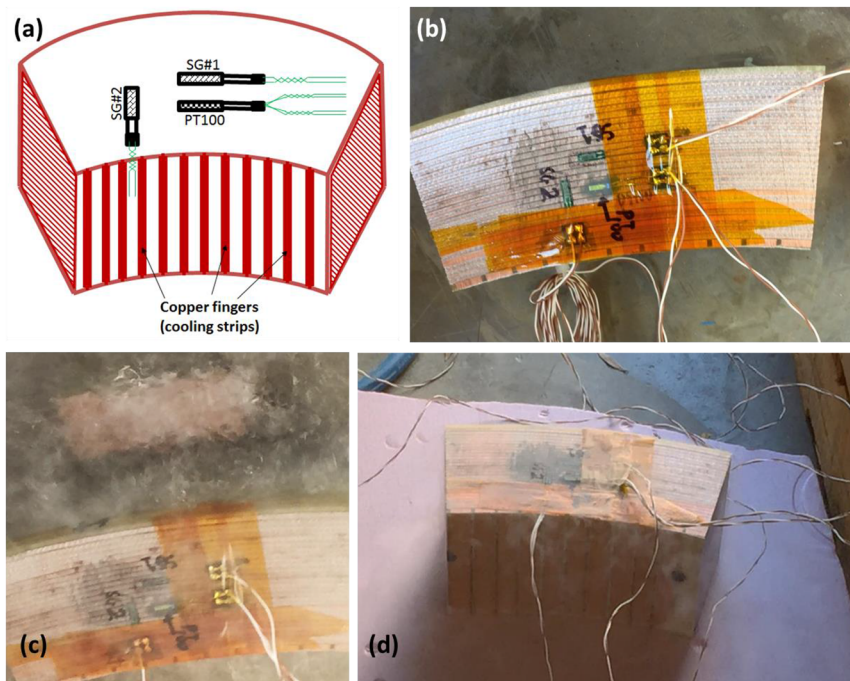
Load cells on the radial and axial supports of the solenoid magnet system were monitored during these tests. No significant changes to the load cell readings were observed during the 19 fast dumps from varying magnet current levels. However, an increase in the solenoid magnet load cell values was observed with increasing current in the torus magnet. With the torus at full field, all load cells read ~400 lbsf higher than when the torus is not powered, as expected from magnet-magnet interaction.[14]

VII. RISK MITIGATION AND APPROACH

Due to the requirement that any in-house developed piece of electronics had to be equivalent to or better than similar commercially available off-the-shelf electronics, a Failure Modes and Effects Analysis (FMEA) process was used to guide and drive the development and final design of the MSELV. FMEA is a tool used to eliminate or mitigate known potential failures, problems, and errors. A failure mode here is defined as the way a component could fail while operating.

JLab utilized the FMEA methodology to identify the highest risk aspects of the MSELV design. The methodology identifies risks and ranks them using a Risk Priority Number (RPN).

This process is limited to failure mitigation from a technical perspective, driving designs that will achieve safe operation of the magnet system employed for the CLAS 12 GeV upgrade in Hall B at JLab.[2] The primary focus has been on system reliability and its adequacy for the proposed design. The criteria of evaluation is based on

FIG. 20. [(a) and (b)] Strain gauge mounting on torus vertical and axial supports and (c) bend test vertical support.

FIG. 22. Two strain gauges and a PT100 temperature sensor mounted on a superconducting coil piece. (a) Diagram showing the locations of sensors on the test section. (b) The test section is wired for hooking up to the trial version of MSELV at room temperature. (c) The test section is immersed in LN2. (d) The test piece is removed from LN2 and warming up to room temperature.
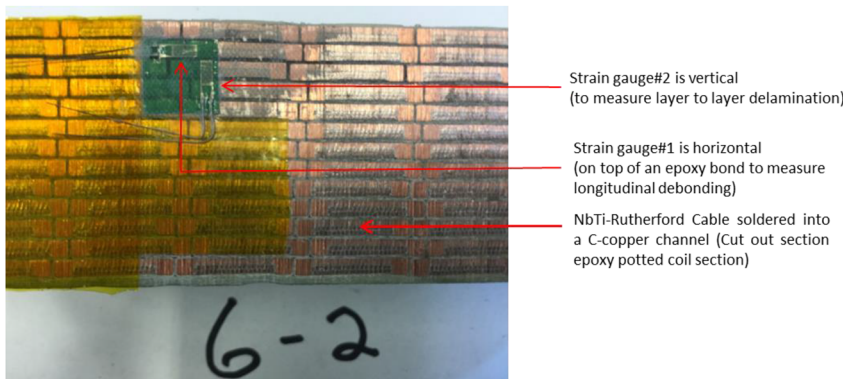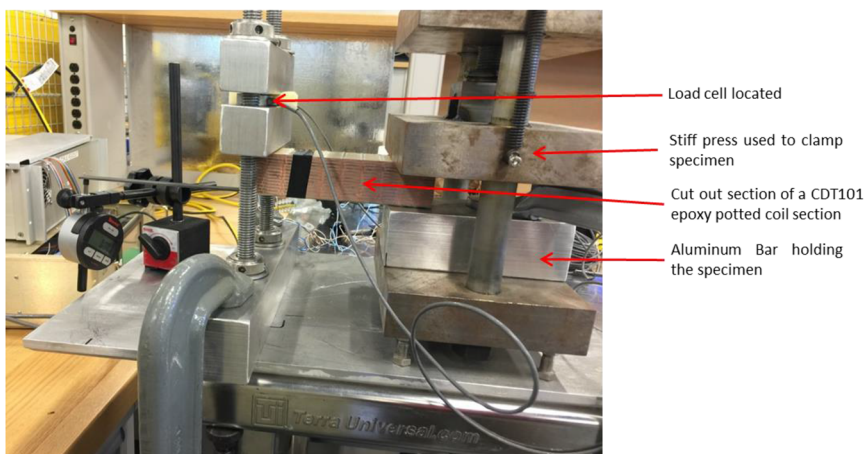
FIG. 23. Strain gauge mounted on an epoxy potted solenoid coil section for strain test using a cantilevered test setup.
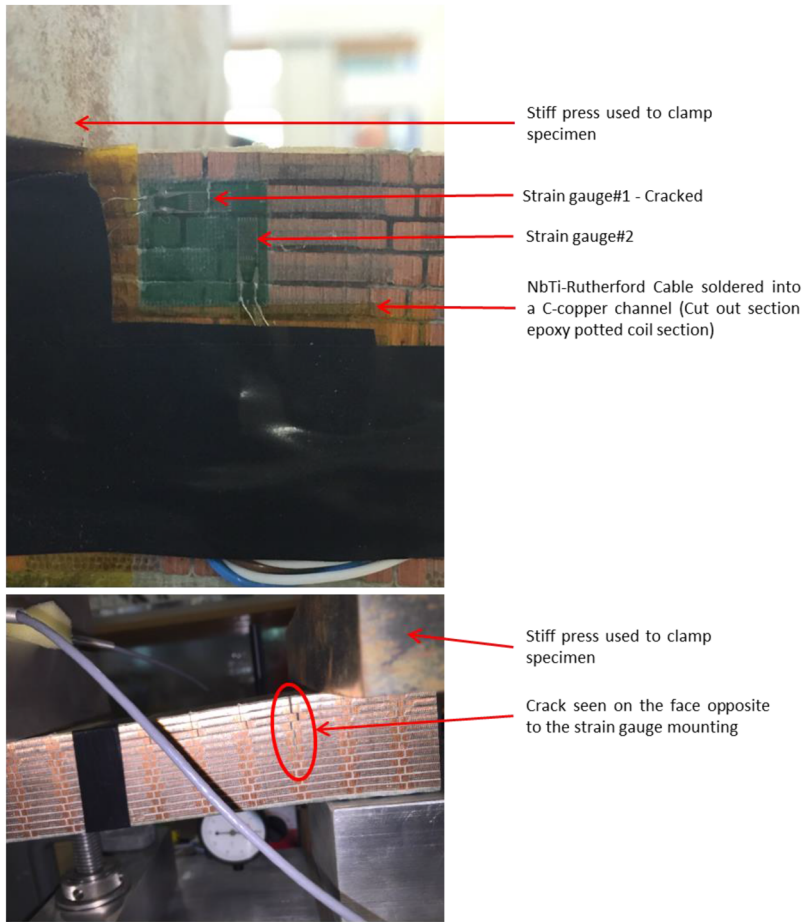
FIG. 24. Cracking and crack propagation on the coil section specimen during the cantilever test.
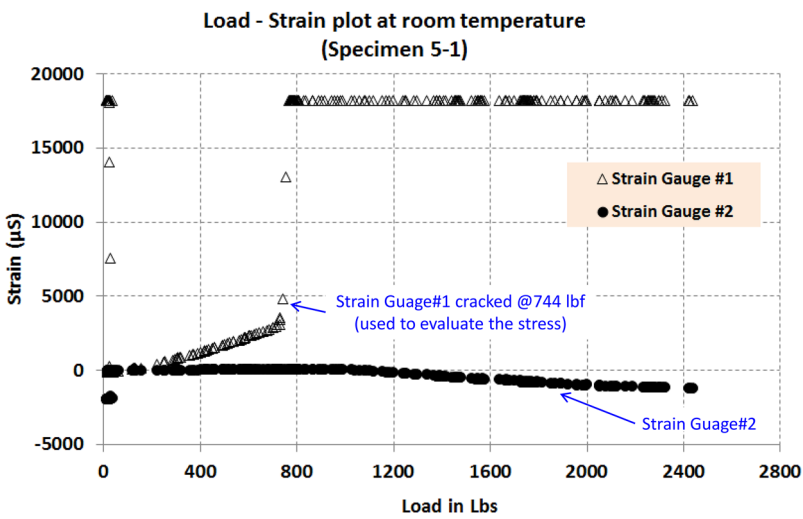
FIG. 25. Strain gauge plot for both strain gauges 1 and 2 (from Fig. 24).

potential failure modes, potential effects of failure, potential causes, and controls that could be put in place together with recommended actions.

A full Failure Modes and Effects Analysis (FMEA) regarding the performance of the MSELV was carried out and a summary of the results is shown below. The FMEA process uses a scoring scale for severity, occurrence, and detection[15] and broadly follows the steps below:

1. For each failure mode, list the possible effects assuming protection devices or logic fail to prevent the failure.
2. Rate the severity of each potential effect. How significant is the impact of the effect, scale 1–6?
3. List the potential causes of the failure mode including failure of the protection device/logic as a cause.
4. Rate the likelihood of occurrence of each cause, scale 1–5.
5. For each potential cause, list the main method for preventing the cause from occurring, detecting that the cause has occurred and/or preventing the failure from continuing from the point that the effects are realized, scale 1–6.
6. Rate the merit of the detection/preventative measures, based on how well do the measures prevent or detect a cause and prevent it from continuing to the point that failure effects will be realized.
7. To calculate the Risk Priority Number (RPN), the highest rated effect that is a logical outcome of each cause and multiply that severity by the likelihood of occurrence and the merit of preventative measures.
8. The failure modes were grouped into three levels by these RPNs: low risk <18, moderate risk <45, and high risk ≥45. For any cause where the RPN is greater than 18, recommend actions to eliminate the cause and/or enhance the prevention and detection.

The risks identified are grouped into four key areas (*firmware, hardware, software, and control*) and are summarized in Fig. 26. The cumulative RPN (in Fig. 27) is simply a summation of all the RPNs for each individual identified risk and provides a top level view of the potential effect of the suggested risk mitigation activities put in place.

One of the highest risks identified was the failure to provide excitation current to the 4 K sensors where the readings are frozen under certain operational and failure modes. A sampling of the identified failure modes is presented in Table IV.

The analysis highlights the changes required in order to make things more reliable and to find the limitations of the MSELV in its present form. This study suggested that the flexibility available with hardware and software to read out many channels quicker (say, 2 kHz) was advantageous and could be used for the fast data acquisition of voltage tap data from the magnet coils and other critical elements such as coil splices. During a magnet engineering run, we encountered a situation where all Cernox sensors on an entire chassis were not responding. The cause of the failure was traced to a failed capacitor on the current source and sense board (Q0131) in the chassis (Fig. 28).

The failed capacitor was a 22 μF, 35 V used for filtering the 12 V-DC input power. When the capacitor failed, it shorted to
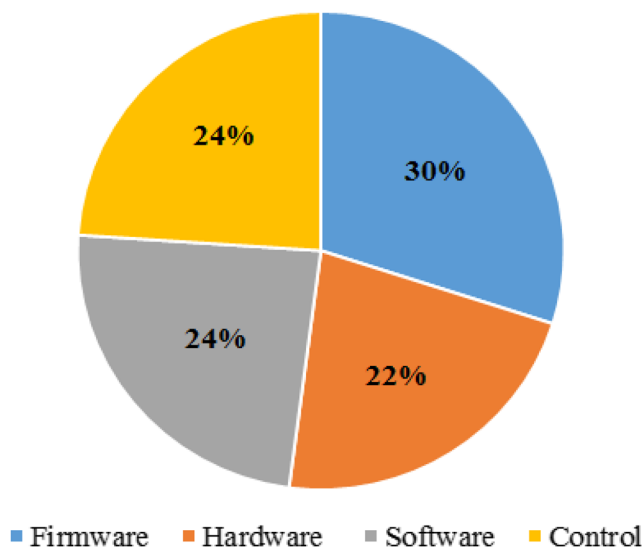
FIG. 26. Segregation of key risks identified (after mitigation/corrective action put into place).

ground causing the onboard fuse to blow. With multiple boards failing in the same way, a detailed study was carried out to see how the sensors would behave with the capacitor removed from the board.

The results are presented by Lemon *et al.*[16] (Table V) and suggests only a 5–6 mK difference between the minimum and maximum values and about 2 mK for the average between two board configurations. This is considered to be insignificant with regards
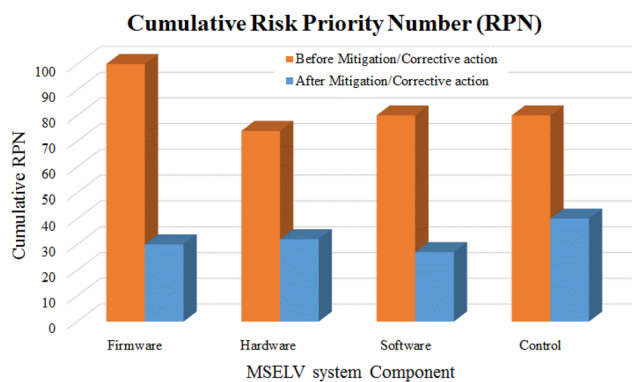
FIG. 27. Cumulative risk priority numbers (before and after mitigation measures are put into place).

TABLE IV. Extract from the FMEA worksheet for the MSELV. SEVERITY (S) = how severe is the effect on the customer; OCCURANCE (O) = how often or frequent; DETECTION (D) = how probable is detection of cause; RPN = S * O * D; RPN-BM is RPN before mitigation; RPN-AM is RPN after mitigation; D (BM) = detection (before mitigation); maximum RPN = 6 (S) * 5 (O) * 6 (D) = 180.

FMEA WORKSHEET - Failure mode and effects analysis

| Potential failure mode	Potential effects of failure	S	Potential causes	O	D (BM)	RPN-BM	Controls could be in place	D	Recommended actions	RPN-AM
Excitation current	Reading coil temperature and control	3	Magnet controlled ramp down	5	4	60	Making the excitation current fixed voltage based rather than fixed power operation	1	Deployed fixed voltage solution	15
Capacitor failure	The whole chassis was down (fuse blown) and could not monitor coil parameters/ could trip the magnet system	4	Normal electrical component failure	3	2	24	Any erratic readout or chassis failure required to replace the chassis with a spare chassis	1	Spare chassis ready for replacement	12
cRIO-serial module failure	All chassis (up to 4) lose communication with PLC	5	Normal component failure	2	2	20	Alarms on loss of communication between cRIO and PLC	1	Spare modules ready for replacement	10
cRIO controller hardware failure	Loss of communications with all LV chassis	5	Loss of power, networking, and normal component failure	3	2	30	Alarms on loss of communication between cRIO and PLC	1	Spare controllers available	15
cRIO controller software failure	Loss of communications with all LV chassis	5	Logic error in code, hardware fault	3	2	30	Additional resets (network, serial, physical) added to system	1	Reboot controller or replace	15
Incorrect calibration tables in cRIO	Loss of accuracy on calibrated sensors	2	Wrong serial number used, calibration data entered incorrectly	2	5	20	Additional review of entered data	3	Additional review of entered data	12
FPGA stops comm. with cRIO	PLC will not receive sensor read back	5	Failure of RS232 interface	1	5	25	Bypassing cRIO, communicate directly with PLC	2	Check the link every second	10
FPGA stops comm. With ADC/DAC	FPGA will not excite sensors and do not receive data from the sensor	5	Buffer chip failure	1	5	25	Inform the cRIO that the data could be corrupted	1	Inform the cRIO the data could be corrupted	5
ADC stops comm. with FPGA	No data from the sensor	5	ADC failure	1	5	25	Alarms on loss of communication	1	Spare board	5
ADC sending erroneous values	Data interpretation will be incorrect	5	Thermal/offset from ADC	1	5	25	Sending a test pattern occasionally to read back	2	As the measurements are differential to minimize the impact	10
DAQ stops comm. with FPGA	No excitation to sensor	5	DAC failure	1	5	25	Sending a test pattern occasionally to read back	2		10
DAQ sets the incorrect excitation current to Cernox	Incorrect excitation	5	Failure of the voltage regulator/current regulator circuit	1	5	25	Reading the return sensor current with ADC	2	Indicate potential problem with excitation to the cRIO/PLC	10
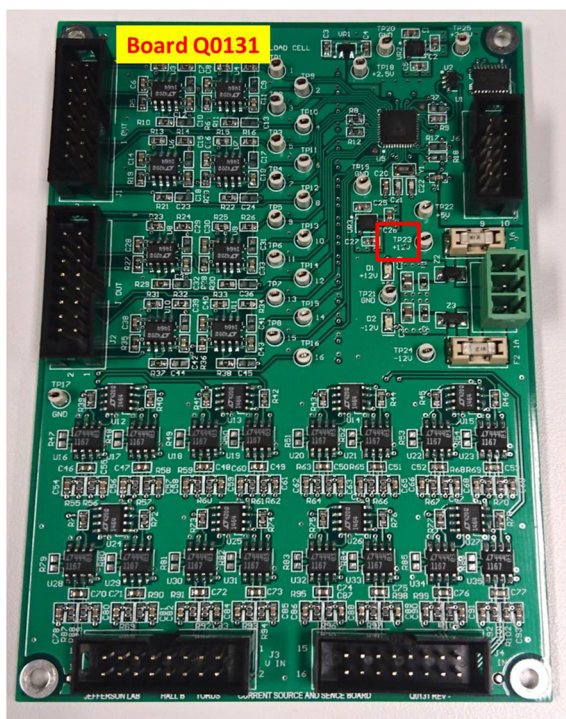
FIG. 28. Board Q0131, with the failed capacitor in the red box.

to the absolute temperature measurement and accuracy and confirmed that the capacitor could indeed be eliminated from the circuit.

As mentioned previously, a total of six MSELV chassis were used to read data from CX, PT100 temperature sensors, load cells, strain gauges, and Hall sensors for the torus magnet system. All the MSELV chassis were connected to two NI-9870 RS232 modules in an NI cRIO controller (LV or slow DAQ cRIO), running LabVIEW. After commissioning and during the engineering run, an unusual problem was observed while reading Cernox sensors, where the temperature reading would suddenly jump to 325 K and remain there. This only happened when the magnet was cold at 4.5 K, as shown in Fig. 29.

Many empirical solutions were tried and tested with 22 errors recorded, as summarized in Tables VI and VII. In order to determine when the 325 K error occurred, indicators were added to the program to monitor the hexadecimal currents sent to Cernox sensors, hexadecimal voltages read from Cernox sensors, and the calculated resistance. The error was discovered, when the two voltages read during a single DAQ loop from a single Cernox were equal. This caused the calculated resistance to be 0.0 Ω and the interpolated temperature to be 325 K (set as default) as in steps 2–8 of Fig. 30.

The error occurred in the version of the LV-cRIO program where the algorithm used to determine Cernox excitation currents targeted a fixed power. The program was modified so that the algorithm instead targets a voltage of 15 mV, i.e., a Fixed Voltage Solution (FVS) as illustrated in Fig. 30 instead of a fixed power

TABLE V. Summary of the temperature reading from the MSELV chassis: (i) with capacitor and (ii) without the capacitor.

Cernox® sensors															
(i) Summary of temperature in K with capacitor (over 86 764 samples)															
	21	22	16	71	12	13	14	15	17	18	19	20			
Minimum	4.655	4.627	5.260	4.748	4.731	4.669	4.666	4.616	4.707	4.636	4.614	4.687			
Maximum	4.791	4.747	5.409	4.852	4.890	4.814	4.801	4.733	4.851	4.765	4.744	4.793			
Average	4.733	4.688	5.341	4.799	4.817	4.751	4.743	4.683	4.785	4.710	4.689	4.749			
Sigma	0.023	0.016	0.024	0.014	0.026	0.023	0.023	0.020	0.022	0.020	0.022	0.018			
(ii) Summary of temperature in K without capacitor (over 92 373 samples)															
Minimum	4.660	4.630	5.265	4.744	4.736	4.677	4.673	4.621	4.718	4.645	4.621	4.693			
Maximum	4.791	4.761	5.424	4.858	4.894	4.815	4.801	4.734	4.855	4.773	4.749	4.797			
Average	4.734	4.689	5.343	4.798	4.818	4.752	4.745	4.685	4.788	4.712	4.691	4.750			
Sigma	0.023	0.017	0.025	0.014	0.026	0.024	0.023	0.020	0.022	0.020	0.023	0.018			

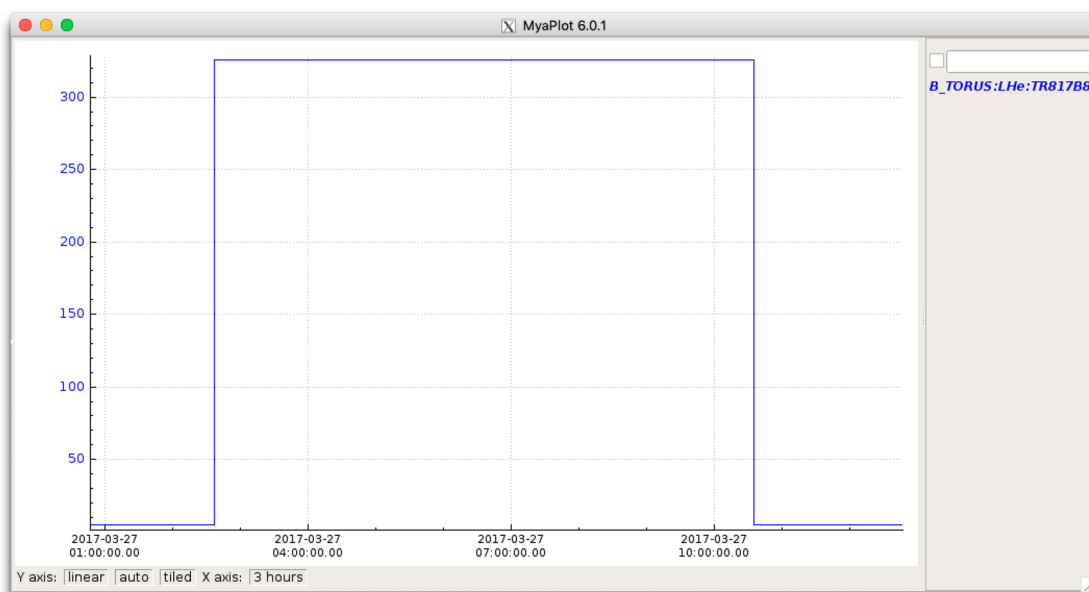|													Overall summary			
Absolute difference of temperature (mK) between data samples in (i) and (ii)													Min.	Max.	Avg.	Sigma
Minimum	5	3	5	4	5	8	7	5	11	9	7	6	3	11	6	2
Maximum	0	15	15	6	4	1	1	1	4	8	4	4	0	15	5	5
Average	1	1	2	1	1	1	2	2	3	2	2	1	1	3	2	1
Sigma	0	1	0	1	0	0	0	0	1	0	0	0	0	1	0	0

FIG. 29. MyaPlot EPICS plot showing a Cernox sensor (TR817B8) jumping to 325 K and staying there until the cRIO program was manually restarted.

solution. This new algorithm is automatically deployed when the MSELV-cRIO starts its initialization routine.

After the FVS was deployed for testing, three instances of a Cernox jumping to 325 K and resuming normal operation after a second were observed. Later, Cernox TR817F9 jumped to 325 K but then resumed normal operation after a second. Constant monitoring of the MSELV-cRIO's program indicated that TR817D3HB1 jumped to 325 K and then resumed normal operation. However, this error and recovery were not recorded in EPICS, and therefore, it was not *decisive* that the FVS was successful. Later, Cernox TR817D3HB1 again jumped to 325 K and resumed normal operation after a second (Fig. 31), confirming that the FVS prevents Cernox sensors from being stuck at 325 K. The most likely cause of the error can be attributed toward fixed power-limited excitation applied across all Cernox sensors that have a wide range of resistance values at ~4 K. The problem was mitigated using the best possible solution that allows an automatic recovery using FVS (not exceeding the recommended power) for the excitation rather than a fixed power excitation as recommended in Table II. These results suggest that the LabVIEW program containing the FVS will successfully deploy automatically any time the cRIO is restarted, thus providing a viable solution.

VIII. SUMMARY AND DISCUSSION

This FPGA-based MSELV Chassis is designed to fulfill the requirement of reading multiple sensors accurately and simultaneously. With the implementation of hardware logic modules with a hardware description language, each control module works independently in a parallel mode, so monitoring and control are significantly improved. By modifying the signal sampling method for

sensors, the measurement speed and accuracy are also significantly improved. The proposed monitoring and control system has been successfully applied on the Hall B torus and solenoid superconducting magnet systems at JLab. The use of the MSELV chassis allowed us to replace multiple racks of equipment, to accommodate various types of readout boxes, and also enabled easier synchronization of the time-stamping of data. We estimated that the use of individual commercially available readout boxes, to accommodate the variety of different sensors, would cost about seven times as much as utilizing the JLab in-house developed MSELV chassis.

A. Cost/economics

A cost comparison was carried out to evaluate the impact of using commercially available off-the-shelf modules/chassis (e.g., temperature readout for Cernox, PT100 sensors, load cell, strain gauge, and Hall sensors) instead of the MSELV, per channel for a typical configuration as shown in Table VIII. The reduction in *cost per channel* employing the MSELV chassis (*consisting of 56 channels per chassis*) has been evaluated to be about 7 times compared to using standard readout boxes with the necessary interfaces to PLC/EPICS.

B. Brief summary of MSELV

1. This instrument readout box is capable of measurement and control (if deployed) for multiple sensors and replaces multiple readout instruments that are normally used to read different sensor types for multiple applications.
2. Read out multiple channels in a synchronous manner.

TABLE VI. List of tasks performed to identify and resolve the error.

Date	Hall B—Torus (log entry No.)	Description	Result
2/2/2017	3 454 964	Developed a procedure for connecting computer to cRIO and manually restarting the cRIO program, which fixed the error.	Manual procedure used to clear error until automatic recovery solution was found.
2/10/2017	3 457 453	Added sub-VI that looks for any Cernox temperature ≥325 K and runs the initialization algorithm just for that sensor. The algorithm attempts to force voltage read from Cernox to be between 0.028 mV and 0.032 mV by varying next iteration's excitation current. After five iterations, Cernox continued its normal operation.	Did not allow the Cernox sensor to recover automatically. The program indicated that the reinitialization algorithm was running in every DAQ loop iteration, when Cernox was at 325 K, but Cernox reading was not affected by the algorithm.
2/20/2017	3 460 573	Swapped LV cRIO module No. 1, NI-9870, with spare. At this point, all errors had been in the MSELV chassis read by module No. 1 so attempted to eliminate the bad module as it was the cause of error.	Additional errors after swapping the module indicated that the module was not the cause of error.
2/28/2017	3 463 259	Added indicators and latching indicators for raw hexadecimal voltages read from the MSELV chassis, raw hexadecimal currents written to MSELV chassis, and resistance as calculated in the program, providing more information when an error occurs. All indicators were also network-shared variables that allowed monitoring without connecting to cRIO. Latching indicators latched when Cernox jumped to 325 K.	For all the cases of error, raw hexadecimal voltages read from MSELV chassis were equal, which caused the calculated resistance to be 0.0 Ω and interpolated temperature to be 325 K. The exact cause of identical voltages is unknown.
4/11/2017	3 469 806	To replicate what happens when the program is manually restarted, a 4 s delay was added after the start-up algorithm runs (see October 2, 2017). During this delay, all VISA communication buffers between LV cRIO and MSELV chassis are cleared.	Delay and VISA clear had no effect on error. On 4/17/2017, delay and VISA clear were removed (*Hall B—Torus Log entry No. 3470177*).
4/21/2017	3 470 593	Added sub-VI for fixed voltage solution to LV-cRIO program.	Three cases were observed, where cernox reading jumping to 325 K and then returning to normal/actual temperature reading after a second later. After the third case, fixed voltage solution was determined to be successful.
6/14/2017	3 475 869	The LV-cRIO program with fixed voltage solution was set as the LV-cRIO's start-up application. This allows cRIO to automatically deploy the program with fixed voltage solution if cRIO is rebooted.	Issue considered resolved.

3. Single firmware provides single and/or multiple excitation to all channels/sensors with a maximum available readout frequency of 23 kHz.
4. Used as a current and voltage source excitation can be provided from nanoamperes to few 100 mA and voltage supply from millivolts to volts with an accuracy better than 1% in the lower range and better than 5% at the upper range.

5. Provides current or voltage excitation to multiple sensors simultaneously.
6. Capable of providing excitation to changing resistances with independent excitation and read back. Passive system—independent of the type of readout and sensor.
7. Capable of measuring high-speed voltage traces (e.g., event of a quench)—not configured presently, but can be added.

TABLE VII. Summary of instances and temperature readout jumping to 325 K (sorted based on the number of errors for each Cernox).

Cernox	Date of error	No. of errors at 325 K	MSELV Chassis No.	MSELV connector	cRIO Module No.	cRIO channel No.
TR817B8	1/24/2017, 2/9/2017, 2/23/2017, 3/27/2017, 4/12/2017	5	4	J6-A	1	3
TR817BR	1/26/2017, 2/11/2017	2	4	J1-A	1	3
TR817F2	2/17/2017, 2/20/2017	2	2	J3-B	1	1
TR817F9	3/30/2017, 4/19/2017[a]	2	2	J6-B	1	1
TR817A2	4/6/2017, 4/19/2017	2	3	J3-B	1	2
TR817D3HB1	5/31/2017,[a] 6/13/2017[a]	2	3	J7-B	1	2
TR8122A	2/2/2017	1	1	J7-A	1	0
TR8122B	1/20/2017	1	1	J7-B	1	0
TR817B7	1/6/2017	1	4	J5-B	1	3
TR817B2	2/10/2017	1	4	J3-B	1	3
TR817B1	3/31/2017	1	4	J3-A	1	3
TR817FS	4/10/2017	1	2	J1-B	1	3
TR817U5HB2	4/16/2017	1	5	J7-B	2	0

[a]325 K errors where the sensor automatically recovered with the fixed voltage solution deployed.
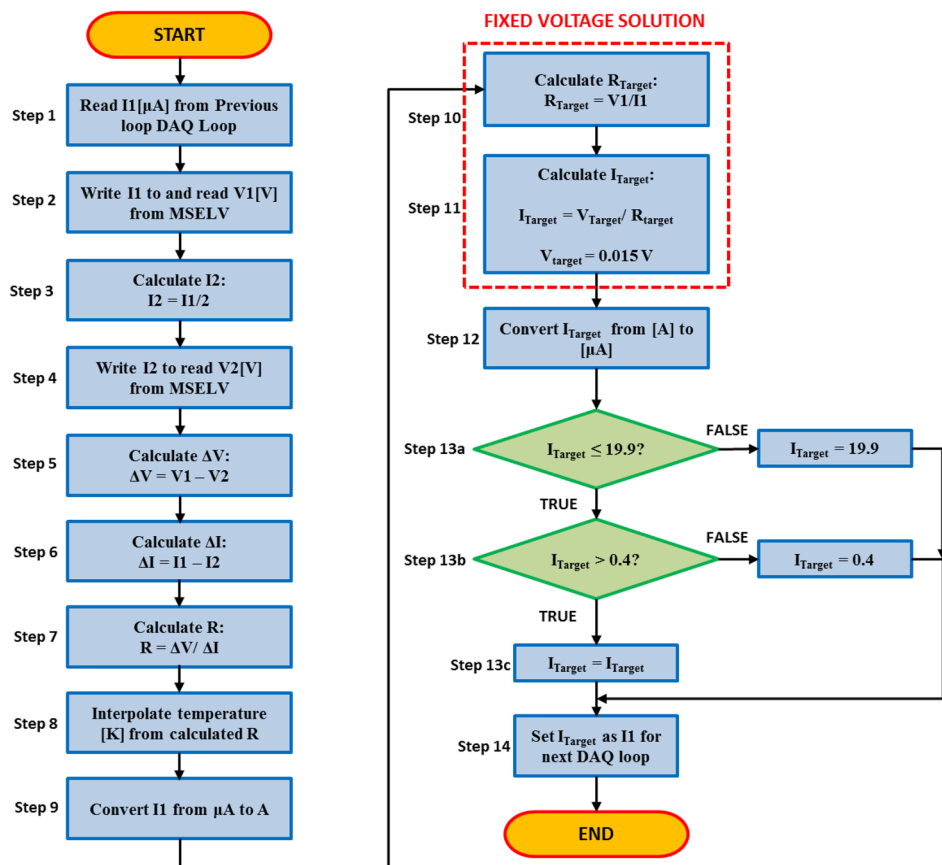
FIG. 30. Flowchart using the fixed voltage solution for Cernox sensor excitation.
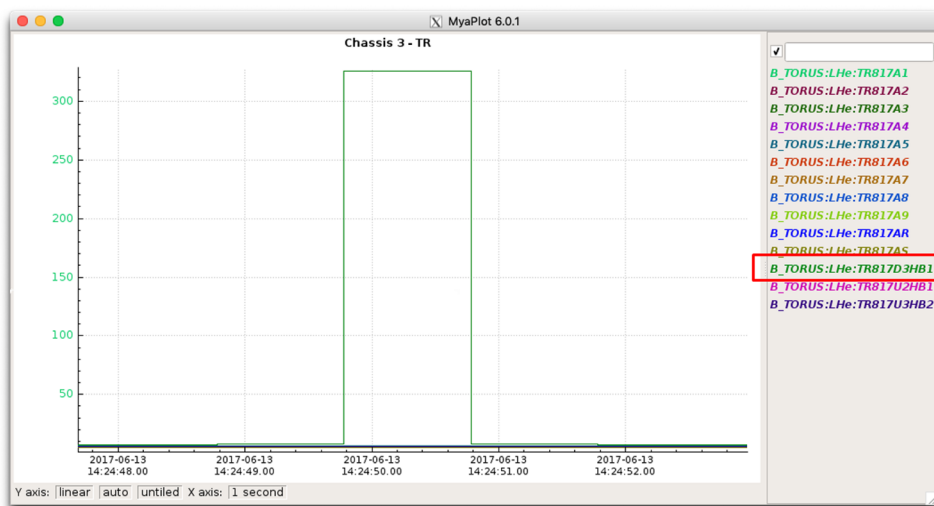
FIG. 31. MyaPlot data from EPICS showing a Cernox sensor (TR817D3HB1) jumping to 325 K and then returning to a normal temperature after a second when utilizing FVS.

TABLE VIII. A typical configuration of MSELV readout channels per chassis.

	Sensor Type						
	PT100	Cernox®	Strain gauges			Load cells[a]/ Hall sensors
Number of channels	2	2	2	2	2	2	2[a]
	2	2	2	2	2	2	2[a]
	2	2	2	2	2	2	2
	2	2	2	2	2	2	2

[a]Load cells

8. Controlled by RS232 or equivalent hardware and power (current or voltage) is independent of the external circuit.
9. Significant reduction in cost per channel.

As mentioned earlier, employing cRIO could be avoided with the upgrade to a FPGA board that runs Linux, which will allow the MSELV to directly communicate with the PLC via EtherNet/IP. Deploying the upgraded FPGA would remove one potential point of failure. This will also open up integration into standard IT-system monitoring and advanced logging.

A system with the operational MSELV chassis within the experimental hall is shown in Fig. 32.
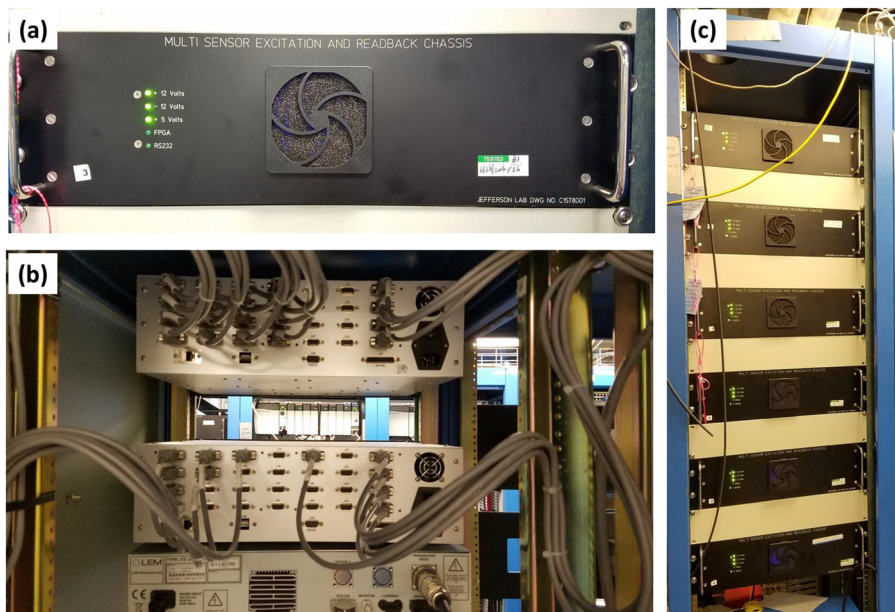

FIG. 32. MSELV within the experimental Hall B: (a) the front panel of the chassis, (b) back panel of the chassis hooked up for the solenoid magnet system, and (c) all 6-chassis showing the front of the panel, part of the torus magnet system.

REFERENCES

[1] R. J. Fair and G. L. Young, IEEE Trans. Appl. Supercond. **25**(3), 4500205 (2015).

[2] P. K. Ghoshal, G. Biallas, R. J. Fair, R. Rajput-Ghoshal, W. Schneider, R. Legg, D. Kashy, J. Hogan, M. Wiseman, C. Luongo, J. Ballard, G. Young, L. Elouadrhiri, and C. Rode, IEEE Trans. Appl. Supercond. **25**(3), 4901005 (2015).

[3] R. Legg, D. Kashy, R. Fair, P. Ghoshal, R. Bachimanchi, K. Bruhwel, M. Taylor, J. Fischer, D. Machie, and J. Powers, IEEE Trans. Appl. Supercond. **25**(3), 4500104 (2015).

[4] P. K. Ghoshal, R. Bachimanchi, R. J. Fair, D. Kashy, R. Rajput-Ghoshal, J. Hogan, N. Sandoval, and G. Young, Supercond. Sci. Technol. **31**, 095007 (2018).

[5] C. Luongo, J. Ballard, G. Biallas, L. Elouadrhiri, R. Fair, P. Ghoshal, D. Kashy, R. Legg, O. Pastor, R. Rajput-Ghoshal, C. Rode, M. Wiseman, G. Young, L. Elementi, S. Krave, A. Makarov, F. Nobrega, and G. Velev, IEEE Trans. Appl. Supercond. **26**(4), 4500105 (2016).

[6] Lakeshore Cryotronics, Cernox Temperature Sensor Technical Data, https://www.lakeshore.com/Documents/LSTC_appendixB_l.pdf, 2017, p. 168.

[7] Texas Instruments, ADS1258-SBAS297G, June 2005, Rev. March 2011, http://www.ti.com/lit/ds/symlink/ads1258.pdf, pp. 13–14.

[8] Designers Guide for Applying Instrument Amplifiers Effectively, http://analog.com/media/en/trainingseminars/design-handbooks/designers-guide-instrument-amps-chV.pdf, pp. 5-12–5-14.

[9] Compact-sized FPGA Development Platform for Prototyping Circuit Designs (DE0_Nano_User_Manual), http://www.terasic.com.tw/cgi-bin/page/archive.pl?Language=English&CategoryNo=139&No=593&PartNo=4.

[10] Single Resistor Gain Programmable Precision Instrumentation Amplifier, www.analog.com/media/en/technicaldocumentation/data-sheets/1167fc.pdf, pp. 16–17.

[11] P. Bonneau, M. A. Antonioli, A. Brown, P. Campero, B. Eng, G. Jacobs, M. Leffel, T. Lemon, M. McMullen, and A. Yegneswaran, Jefferson Lab DSG Note No. 2019-53 (2019), https://www.jlab.org/div_dept/physics_division/dsg/notes/2019-37%20FPGA%20Upgrade%20Proposals%20for%20the%20Hall%20B%20Torus%20and%20Solenoid%20Control%20and%20Monitoring%20Systems.pdf.

[12] See http://www.futek.com/application/load-cell for information about FUTEK FSH02239.

[13] See https://tml.jp/e/product/strain_gauge/cf_list.html for Cryogenic compatible Strain gauges (CF series both Single & Rosette plane type).

[14] R. Rajput-Ghoshal, P. K. Ghoshal, R. J. Fair, J. Hogan, and D. Kashy, IEEE Trans. Appl. Supercond. **25**(3), 4100605 (2015).

[15] P. K. Ghoshal, D. Chavez, R. J. Fair, S. Gopinath, D. H. Kashy, P. McIntyre, T. Michalski, R. Rajput-Ghoshal, and A. Sattarov, IEEE Trans. Appl. Supercond. **30**(1), 4700211 (2020).

[16] T. Lemon, M. A. Antonioli, S. Arslan, P. Bonneau, P. Campero, B. Eng, A. Hoebel, G. Jacobs, M. Leffel, M. McMullen, and A. Yegneswaran, Jefferson Lab DSG Note No. 2017-06 (2017), https://www.jlab.org/div_dept/physicsdivision/dsg/notes/2017-06%20Torus%20Cernox%20325%20K%20error.pdf.